Available online at www.sciencedirect.com
ScienceDirect
International Journal of Thermal Sciences 48 (2009) 891–912
International Journal of Thermal Sciences
www.elsevier.com/locate/ijts

Analysis of mixed convection flows within a square cavity with uniform and non-uniform heating of bottom wall

Tanmay Basak [a], S. Roy [b], Pawan Kumar Sharma [b], I. Pop [c,*]

[a] *Department of Chemical Engineering, Indian Institute of Technology Madras, Chennai 600036, India*
[b] *Department of Mathematics, Indian Institute of Technology Madras, Chennai 600036, India*
[c] *Faculty of Mathematics, University of Cluj, R-3400 Cluj, CP 253, Romania*

Received 9 April 2008; received in revised form 7 August 2008; accepted 7 August 2008

Available online 10 September 2008

Abstract

A penalty finite element analysis with bi-quadratic elements is performed to investigate the influence of uniform and non-uniform heating of bottom wall on mixed convection lid driven flows in a square cavity. In the present investigation, bottom wall is uniformly and non-uniformly heated while the two vertical walls are maintained at constant cold temperature and the top wall is well insulated and moving with uniform velocity. A complete study on the effect of Gr shows that the strength of circulation increases with the increase in the value of Gr irrespective of Re and Pr. As the value of Gr increases, there occurs a transition from conduction to convection dominated flow at $Gr = 5 \times 10^3$ and $Re = 1$ for $Pr = 0.7$. A detailed analysis of flow pattern shows that the natural or forced convection is based on both the parameters Ri ($\frac{Gr}{Re^2}$) and Pr. As the value of Re increases from 1 to 10^2, there occurs a transition from natural convection to forced convection depending on the value of Gr irrespective of Pr. Particularly for higher value of Grashof number ($Gr = 10^5$), the effect of natural convection is dominant upto $Re = 10$ and thereafter the forced convection is dominant with further increase in Re. As Pr increases from 0.015 to 10 for a fixed Re and Gr ($Gr = 10^3$), the inertial force gradually becomes stronger and the intensity of secondary circulation gradually weakens. The local Nusselt number (Nu_b) plot shows that the heat transfer rate is very high at the edges of the bottom wall and then decreases at the center of the bottom wall for the uniform heating and that contrasts lower heat transfer rate at the edges for the non-uniform heating of the bottom wall. It is also observed that Nu_l shows non-monotonic behavior with both uniform and non-uniform heating cases for $Re = 10$ at higher value of Pr. The average Nusselt number plot for the left or right wall shows a kink or inflexion at $Gr = 10^4$ for highest value of Pr. Thus the overall power law correlation for average Nusselt number may not be obtained for mixed convection effects at higher Pr.

Keywords: Mixed convection; Square cavity; Uniform and non-uniform heating; Penalty finite element method

1. Introduction

A convection situation involving both natural and forced convection is commonly referred as mixed convection. In mixed convection flows, the forced convection as well as the free convection effects are of comparable magnitudes. Thus, mixed convection occurs if the effect of buoyancy forces on a forced flow or the effect of forced flow on a buoyant flow is significant. The governing non-dimensional parameters for the description of flows are Grashof number (Gr), Reynolds number (Re) and Prandtl number (Pr). In addition, another dimensionless parameter, Richardson number (Ri) may be defined as $Ri = Gr/Re^n$. Analysis indicates that Richardson number (Ri) characterizes mixed convection flow where Gr and Re represent the strength of the natural and forced convection flow effects, respectively. The limiting case $Ri \to 0$ and $Ri \to \infty$ correspond to the forced and natural convection flows, respectively. The exponent n depends on the geometry, thermal boundary condition and the fluid. Bejan [1] carried out a scale analysis of mixed convection flow over a vertical wall and showed that the criterion for the transition from the forced convection dominant flow to natural convection dominant flow was not the same for fluids with

* Corresponding author.
E-mail addresses: tanmay@iitm.ac.in (T. Basak), sjroy@iitm.ac.in (S. Roy), pop.ioan@yahoo.co.uk (I. Pop).

1290-0729/$ – see front matter
doi:10.1016/j.ijthermalsci.2008.08.003

Nomenclature

g	acceleration due to gravity	$m\,s^{-2}$
J	Jacobian of Residual equations	
k	thermal conductivity	$W\,m^{-1}\,K^{-1}$
L	length of the square cavity	m
N	total number of nodes	
Nu	local Nusselt number	
p	pressure	Pa
P	dimensionless pressure	
Pr	Prandtl number	
R	Residual of weak form	
Re	Reynolds number	
Gr	Grashof number	
T	temperature	K
T_h	temperature of hot bottom wall	K
T_c	temperature of cold side walls	K
u	x component of velocity	$m\,s^{-1}$
U	X component of dimensionless velocity	
U_0	velocity of the upper lid in x-direction	$m\,s^{-1}$
v	y component of velocity	$m\,s^{-1}$
V	Y component of dimensionless velocity	
X	dimensionless distance along x-coordinate	
Y	dimensionless distance along y-coordinate	

Greek symbols

α	thermal diffusivity	$m^2\,s^{-1}$
β	volume expansion coefficient	K^{-1}
γ	penalty parameter	
θ	dimensionless temperature	
ν	kinematic viscosity	$m^2\,s^{-1}$
ρ	density	$kg\,m^{-3}$
Φ	basis functions	
ψ	stream function	

Subscripts

b	bottom wall
i	residual number
k	node number
s	side wall

Superscripts

n	Newton iterative index

$Pr \geqslant 1$ and $Pr \leqslant 1$. The transition criterion is not yet validated for $Pr \ll 1$ due to non-existence of experimental data for this range of Pr.

Mixed convection problem with lid driven flows within an enclosure finds a wide range of applications in various fields of engineering and science such as flow and heat transfer in solar ponds [2], dynamics of lakes [3], thermal-hydraulics of nuclear reactors [4] and float glass production [5]. The lid driven cavity problem has been extensively used as a benchmark case for the evaluation of numerical solution algorithms [6,7].

Previous studies reflect that there are two categories of study available for mixed convection flows in enclosures. The first category is concerned with a horizontal sliding lid which encompasses the top wall [8–12], bottom sliding wall [13,14] or an oscillating lid [15,16]. These studies have been extended for three dimensional cavities [17,18]. The other type of problem is associated with side driven differentially-heated enclosures, where one wall or both vertical walls move with a constant velocity in their planes [19–21].

Moallemi and Jang [8] analyzed the effects of Prandtl number (Pr) on laminar mixed convection heat transfer in a lid driven cavity. They performed the numerical simulations for two-dimensional laminar flow ($100 \leqslant Re \leqslant 2200$) and studied the effects of small to moderate Prandtl numbers ($0.01 \leqslant Pr \leqslant 50$) on the flow and heat transfer characteristics in a square cavity for various values of Richardson number (Ri). The temperature and flow fields in the cavity show the strong influence of Prandtl number, Pr. The local and average Nusselt numbers are also reported for various values of Re, Ri and Pr. Mixed convection heat transfer in a lid driven cavity was also investigated by Prasad and Koseff [9]. They performed a series of experiments in a cavity filled with water and measured the heat flux at different locations over the hot cavity floor for a range of Re and Gr. Their results indicate that the overall (i.e. area averaged) heat transfer rate is a very weak function of Gr for $2200 \leqslant Re \leqslant 12000$.

A significant amount of mixed convection studies involve various applications. Mohamad and Viskanta [10] reported on the onset of instability in a shallow lid-driven cavity heated from below. They carried out a linear stability analysis and found that Pr influences the conditions for the initiation of the mixed convection regime. Amiri et al. [11] have analyzed the effects of mixed convection heat transfer in lid driven cavity with sinusoidal wavy bottom surface. They investigated the implications of Richardson number (Ri), number of wavy surface undulations, and amplitude of wavy surface on the flow structure for $Pr = 1$. They have also illustrated that the average Nusselt number increases with an increase in both amplitude of the wavy surface and Reynolds number (Re).

Oztop and Dagtekin [21] studied steady state two-dimensional mixed convection problem in a vertical two-sided lid-driven differentially heated square cavity. The left and right moving walls were maintained at different constant temperatures while upper and bottom walls were thermally insulated. Three cases were considered depending on the direction of moving walls and Richardson number, Ri. They observed that both Richardson number and direction of moving walls affect the fluid flow and heat transfer in the cavity. For $Ri \leqslant 1$, the influence of moving walls on the heat transfer is the same when the walls move in opposite direction regardless of which side moving upwards and the influence is less when both sides move upwards. For the case of opposing buoyancy and shear forces and for $Ri \geqslant 1$, the heat transfer rate is larger due to formation

of secondary cells on the walls and a counter rotating cell at the center.

A few applications on mixed convection involve in channels within open cavity [22–24]. Manca et al. [22] studied numerically mixed convection in an open cavity with a heated wall bounded by a horizontally insulated plate. They considered three basic heating modes: (i) the heated wall is on the inflow side (assisting flow); (ii) the heated wall is on the outflow side (opposing flow); and (iii) the heated wall is the horizontal surface of the cavity (heating from below). Their results are reported based on streamlines, isotherms, wall temperature, and the velocity profiles. They found that the opposing forced flow configuration has the highest thermal performance in terms of both maximum temperature and average Nusselt number. Later, Manca et al. [23] carried out experimental investigations on mixed convection in an open cavity with a heated wall on the inflow side, bounded by a horizontally unheated plate. The flow visualization illustrates two nearly distinct fluid motions for $Re = 1000$: a parallel forced flow in the channel and a recirculation flow inside the cavity. They found that the effect of a stronger buoyancy determines a penetration of thermal plume front for $Re = 100$. Their experimental investigation was further extended for mixed convection in an open cavity with a heated wall bounded by a horizontal unheated plate where the heated wall is on the opposite side of the forced inflow [24].

Mixed convection studies are also carried out in presence of isolated or discrete heat sources [25–27]. Papanicolaou and Jaluria [25] studied the effects of mixed convection from an isolated heat source in a rectangular enclosure. Their study is based on the mixed convection transport from an isolated thermal source, with a uniform surface heat flux input and located in a rectangular enclosure. The interaction of the cooling stream with the buoyancy-induced flow from the heat source is of interest in this work. Laminar, two-dimensional flow is assumed, and the problem lies in the mixed convection regime, governed by the buoyancy parameter ($\frac{Gr}{Re^2}$) and the Reynolds number (Re).

Hsu et al. [26] studied combined free and forced convection in a partially divided enclosure with a finite-size heat source. The enclosure is partially divided by a conductive vertical divider protruding from the floor or the ceiling of the enclosure. The present study simulates a practical system such as air-cooled electronic equipment with heated components. The developed mathematical model is governed by the coupled equations of stream function, vorticity transport, and energy and is solved by employing the cubic spline collocation scheme. The results indicate that the average Nusselt number and the dimensionless surface temperature on the heat source strongly depend on the location and the height of the divider.

Hsu and Wang [27] carried out numerical study on mixed convective heat transfer in rectangular enclosure. The discrete heat sources are embedded on a vertical board, which is situated on the bottom wall of an enclosure. An external airflow enters the enclosure through an opening in one vertical wall and exits from another opening in the opposite wall. This study simulates a practical system, such as air-cooled electronic devices with heated elements. The computational results indicate that both the thermal field and the average Nusselt number ($\overline{Nu}$) depend strongly on the governing parameters, position of the heat sources, as well as the property of the heat-source-embedded board. Although there are a number of studies available in the literature as mentioned above for mixed convection flows within enclosures, the detailed analysis on local and average heat transfer rates as a function of various governing parameters is yet to appear in the literature.

Current study deals with the mixed convection heating of commonly used liquids in a square enclosure where the bottom wall is heated (uniformly and non-uniformly) and vertical walls are exposed to cooled ambiance whereas the lid driven top wall is well insulated and sliding with a uniform velocity. It may be noted that present study stems from a recent work [28] where natural convection within a square cavity has been investigated in presence of uniform and non-uniform heating of the bottom wall. The flow circulations, isotherms and Nusselt number have been reported for $10^3 \leqslant Ra \leqslant 10^5$ with $Pr = 0.7$–10. The critical Rayleigh numbers for conduction dominant regimes have also been found for the uniform and non-uniform heating cases. Overall, the article [28] analyzes natural convection effects which correspond to $Ri = \infty$ and thus current work focuses mainly on mixed convection regime.

The aim of the present paper is to provide a complete understanding about the problem, solution procedure using finite element method and detailed analysis of temperature and the flow fields on heat transfer evaluation. In the current study, Galerkin finite element [29] method with penalty parameter has been used to solve the nonlinear coupled partial differential equations governing flow and temperature fields for both uniform and sinusoidally varying temperature distribution prescribed at bottom wall. The detailed analysis of heat transfer rates or Nusselt numbers has been carried out using finite element basis functions.

2. Problem formulation

A two-dimensional square cavity is considered for the present study with the physical dimension as shown in Fig. 1. The bottom wall of the cavity is maintained at a uniform or non-uniform temperature and the upper wall is insulated. The two vertical walls are maintained at cold temperature. It may be noted that the bottom wall is maintained at a higher temperature to induce buoyancy effect. The top wall is assumed to slide from left to right with a constant speed U_0. The flow is assumed to be laminar and the fluid properties are assumed to be constant except for the density variation which is modeled according to Boussinesq approximation while viscous dissipation effects are considered to be negligible. The viscous incompressible flow and the temperature distribution inside the cavity are governed by the Navier–Stokes and the energy equations, respectively. The aim of the current work is to investigate the steady solutions and hence, we have considered the time independent differential equations. Similar procedure was also followed in the recent work on mixed convection [11]. A number of earlier works was based on steady solutions which were

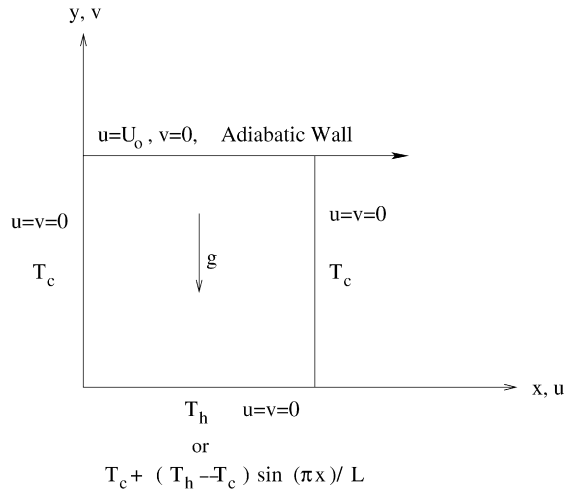

Fig. 1. Schematic diagram of the physical system.

obtained via steady mathematical model [8–10,28,31,33]. The governing equations are non-dimensionalized to yield

$$\frac{\partial U}{\partial X}+\frac{\partial V}{\partial Y}=0 \tag{1}$$

$$U\frac{\partial U}{\partial X}+V\frac{\partial U}{\partial Y}=-\frac{\partial P}{\partial X}+\frac{1}{Re}\left(\frac{\partial^2 U}{\partial X^2}+\frac{\partial^2 U}{\partial Y^2}\right) \tag{2}$$

$$U\frac{\partial V}{\partial X}+V\frac{\partial V}{\partial Y}=-\frac{\partial P}{\partial Y}+\frac{1}{Re}\left(\frac{\partial^2 V}{\partial X^2}+\frac{\partial^2 V}{\partial Y^2}\right)+\frac{Gr}{Re^2}\theta \tag{3}$$

$$U\frac{\partial \theta}{\partial X}+V\frac{\partial \theta}{\partial Y}=\frac{1}{Re\,Pr}\left(\frac{\partial^2 \theta}{\partial X^2}+\frac{\partial^2 \theta}{\partial Y^2}\right) \tag{4}$$

The transformed boundary conditions are:

$$U(X,1)=1,\qquad U(X,0)=U(0,Y)=U(1,Y)=0$$
$$V(X,0)=V(X,1)=V(0,Y)=V(1,Y)=0$$
$$\theta(X,0)=1 \quad \text{or} \quad \sin(\pi X)$$
$$\theta(0,Y)=\theta(1,Y)=0,\qquad \frac{\partial \theta}{\partial Y}(X,1)=0 \tag{5}$$

The dimensionless variables and parameters are defined as follows:

$$X=\frac{x}{L},\quad Y=\frac{y}{L},\quad U=\frac{u}{U_0}$$
$$V=\frac{v}{U_0},\quad \theta=\frac{T-T_c}{T_h-T_c},\quad P=\frac{p}{\rho U_0^2}$$
$$Pr=\frac{\nu}{\alpha},\quad Re=\frac{U_0 L}{\nu},\quad Gr=\frac{g\beta(T_h-T_c)L^3}{\nu^2} \tag{6}$$

Here x and y are the distances measured along the horizontal and vertical directions, respectively; u and v are the velocity components in x- and y-directions, respectively; T denotes the temperature; p is the pressure and ρ is the density; T_h and T_c are the temperature at the hot and cold walls, respectively; L is the length of the side of the square cavity; X and Y are dimensionless coordinates varying along horizontal and vertical directions, respectively; U_0 is the velocity of the upper wall; U and V are dimensionless velocity components in the X and Y directions, respectively; θ is the dimensionless temperature; P is the dimensionless pressure; Gr, Re and Pr are Grashof, Reynolds and Prandtl number, respectively.

3. Solution procedure

The momentum and energy balance equations [Eqs. (2)–(4)] are the combinations of mixed elliptic–parabolic system of equations which have been solved using the Galerkin finite element method. The continuity equation [Eq. (1)] have been used as a constraint due to mass conservation and this constraint may be used to obtain the pressure distribution. In order to solve Eqs. (2)–(3), we use the penalty finite element method where the pressure P is eliminated by a penalty parameter γ and the incompressibility criteria given by Eq. (1) (see [29]) results in

$$P=-\gamma\left(\frac{\partial U}{\partial X}+\frac{\partial V}{\partial Y}\right) \tag{7}$$

The continuity equation [Eq. (1)] is automatically satisfied for large values of γ. Typical values of γ that yield consistent solutions are 10^7. Using Eq. (7), the momentum balance equations [Eqs. (2) and (3)] reduce to

$$U\frac{\partial U}{\partial X}+V\frac{\partial U}{\partial Y}=\gamma\frac{\partial}{\partial X}\left(\frac{\partial U}{\partial X}+\frac{\partial V}{\partial Y}\right)+\frac{1}{Re}\left(\frac{\partial^2 U}{\partial X^2}+\frac{\partial^2 U}{\partial Y^2}\right) \tag{8}$$

and

$$U\frac{\partial V}{\partial X}+V\frac{\partial V}{\partial Y}=\gamma\frac{\partial}{\partial Y}\left(\frac{\partial U}{\partial X}+\frac{\partial V}{\partial Y}\right)+\frac{1}{Re}\left(\frac{\partial^2 V}{\partial X^2}+\frac{\partial^2 V}{\partial Y^2}\right)+\frac{Gr}{Re^2}\theta \tag{9}$$

The system of equations [Eqs. (4), (8) and (9)] with boundary conditions [Eq. (5)] are solved by using Galerkin finite element method [29]. Expanding the velocity components (U, V) and temperature (θ) using basis set $\{\Phi_k\}_{k=1}^N$ as,

$$U\approx\sum_{k=1}^{N}U_k\Phi_k(X,Y)$$
$$V\approx\sum_{k=1}^{N}V_k\Phi_k(X,Y),\quad \text{and}$$
$$\theta\approx\sum_{k=1}^{N}\theta_k\Phi_k(X,Y) \tag{10}$$

the Galerkin finite element method yields the following nonlinear residual equations for Eqs. (8), (9) and (4), respectively, at nodes of internal domain Ω:

$$R_i^{(1)}=\sum_{k=1}^{N}U_k\int_{\Omega}\left[\left(\sum_{k=1}^{N}U_k\Phi_k\right)\frac{\partial\Phi_k}{\partial X}+\left(\sum_{k=1}^{N}V_k\Phi_k\right)\frac{\partial\Phi_k}{\partial Y}\right]\Phi_i\,dX\,dY$$

$$+\gamma\left[\sum_{k=1}^{N} U_k \int_{\Omega} \frac{\partial \Phi_i}{\partial X}\frac{\partial \Phi_k}{\partial X}\,dX\,dY + \sum_{k=1}^{N} V_k \int_{\Omega} \frac{\partial \Phi_i}{\partial X}\frac{\partial \Phi_k}{\partial Y}\,dX\,dY\right] + \frac{1}{Re}\sum_{k=1}^{N} U_k \int_{\Omega}\left[\frac{\partial \Phi_i}{\partial X}\frac{\partial \Phi_k}{\partial X} + \frac{\partial \Phi_i}{\partial Y}\frac{\partial \Phi_k}{\partial Y}\right] dX\,dY \quad (11)$$

$$R_i^{(2)} = \sum_{k=1}^{N} V_k \int_{\Omega}\left[\left(\sum_{k=1}^{N} U_k \Phi_k\right)\frac{\partial \Phi_k}{\partial X} + \left(\sum_{k=1}^{N} V_k \Phi_k\right)\frac{\partial \Phi_k}{\partial Y}\right]\Phi_i\,dX\,dY + \gamma\left[\sum_{k=1}^{N} U_k \int_{\Omega} \frac{\partial \Phi_i}{\partial Y}\frac{\partial \Phi_k}{\partial X}\,dX\,dY + \sum_{k=1}^{N} V_k \int_{\Omega} \frac{\partial \Phi_i}{\partial Y}\frac{\partial \Phi_k}{\partial Y}\,dX\,dY\right] + \frac{1}{Re}\sum_{k=1}^{N} V_k \int_{\Omega}\left[\frac{\partial \Phi_i}{\partial X}\frac{\partial \Phi_k}{\partial X} + \frac{\partial \Phi_i}{\partial Y}\frac{\partial \Phi_k}{\partial Y}\right] dX\,dY + \frac{Gr}{Re^2}\int_{\Omega}\left(\sum_{k=1}^{N}\theta_k \Phi_k\right)\Phi_i\,dX\,dY \quad (12)$$

and

$$R_i^{(3)} = \sum_{k=1}^{N} \theta_k \int_{\Omega}\left[\left(\sum_{k=1}^{N} U_k \Phi_k\right)\frac{\partial \Phi_k}{\partial X} + \left(\sum_{k=1}^{N} V_k \Phi_k\right)\frac{\partial \Phi_k}{\partial Y}\right]\Phi_i\,dX\,dY + \frac{1}{Re\,Pr}\sum_{k=1}^{N} \theta_k \int_{\Omega}\left[\frac{\partial \Phi_i}{\partial X}\frac{\partial \Phi_k}{\partial X} + \frac{\partial \Phi_i}{\partial Y}\frac{\partial \Phi_k}{\partial Y}\right] dX\,dY. \quad (13)$$

The set of non-linear algebraic equations [Eqs. (11)–(13)] are solved using reduced integration technique [29,30] and Newton–Raphson method as discussed in earlier work [28,31]. The numerical solutions obtained in terms of the velocity components (U, V) and stream functions (ψ) are evaluated using the relationship between the stream function (ψ) and the velocity components [32], where the stream function (ψ) is defined in the usual way as $U = \frac{\partial \psi}{\partial Y}$ and $V = -\frac{\partial \psi}{\partial X}$. It may be noted that, the positive sign of ψ denotes anti-clockwise circulation and the clockwise circulation is represented by the negative sign of ψ. The no-slip condition is valid at all boundaries as there is no cross flow, hence $\psi = 0$ is used for the boundaries except for the moving top wall. The heat transfer coefficient in terms of the local Nusselt number (Nu) is defined by

$$Nu = -\frac{\partial \theta}{\partial n} \quad (14)$$

where n denotes the normal direction on a plane. The local Nusselt numbers at bottom wall (Nu_b) and at the side wall (Nu_s) are defined as:

$$Nu_b = -\sum_{i=1}^{9} \theta_i \frac{\partial \Phi_i}{\partial Y} \quad (15)$$

and

$$Nu_s = -\sum_{i=1}^{9} \theta_i \frac{\partial \Phi_i}{\partial X} \quad (16)$$

The average Nusselt numbers at the bottom and side walls are:

$$\overline{Nu_b} = \frac{\int_0^1 Nu_b\,dX}{X|_0^1} = \int_0^1 Nu_b\,dX \quad (17)$$

and

$$\overline{Nu_s} = \frac{\int_0^1 Nu_s\,dY}{Y|_0^1} = \int_0^1 Nu_s\,dY \quad (18)$$

Note that, $\overline{Nu_s}$ may be referred as $\overline{Nu_l}$ and $\overline{Nu_r}$ for the left and right walls, respectively.

4. Results and discussion

4.1. Numerical tests

The computational domain consists of 20×20 bi-quadratic elements which correspond to 41×41 grid points. The bi-quadratic elements with lesser number of nodes smoothly capture the non-linear variations of the field variables which are in contrast with finite difference/finite volume solution available in the literature [21]. In order to assess the accuracy of our numerical procedure, we have also tested our algorithm based on the grid size for driven cavity flow [6] and mixed convection [8].

Numerical solutions are obtained for various values of $Gr = 10^3$–10^5, $Pr = 0.015$–10 and $Re = 1$–10^2 with uniform and non-uniform heating of the bottom wall where the two vertical walls are cooled and the top wall is well insulated with a horizontal velocity, $U = 1$. The jump discontinuity in Dirichlet type of wall boundary conditions at the corner point (see Fig. 1) corresponds to computational singularity. To ensure the convergence of the numerical solution to the exact solution, the grid sizes have been optimized and the results presented here are independent of grid sizes. In particular, the singularity at the corner nodes of the bottom wall needs special attention. The grid size dependence effect of the temperature discontinuity at the corner points upon the local and average Nusselt numbers tend to increase as the mesh spacing at the corner is reduced. One of the ways for handling the problem is assuming the average temperature of the two walls at the corner and keeping the adjacent grid-nodes at the respective wall temperatures. Alternatively, based on earlier work by Ganzarolli and Milanez [33], this procedure is still grid dependent unless a sufficiently refined mesh is implemented. Accordingly, once any

corner formed by the intersection of two differentially heated boundary walls is assumed at the average temperature of the adjacent walls, the optimal grid size obtained for each configuration corresponds to the mesh spacing over which further grid refinements lead to grid invariant results in both heat transfer rates and flow fields.

In the current investigation, Gaussian quadrature based finite element method provides the smooth solutions at the interior domain including the corner regions as evaluation of residual depends on interior Gauss points and thus the effect of corner nodes is less pronounced in the final solution. The present finite element approach offers special advantage on evaluation of local Nusselt number at the bottom and side walls as the element basis functions are used to evaluate the heat flux. The numerical accuracy on the average Nusselt numbers and maximum horizontal and vertical dimensionless velocity components at an assigned vertical and horizontal plane across the cavity are within 0.1–1%.

4.2. Effect of Grashof number: uniform and non-uniform heating of the bottom wall

Figs. 2–4 illustrate the stream function and isotherm contours with the uniformly heated bottom wall for $Gr = 10^3$–10^5, $Pr = 0.015$–10 and $Re = 1$. Fig. 2(a) shows that the effect of lid-driven flow predominates the natural convection for $Gr = 10^3$ and $Pr = 0.015$. The lid velocity produces inertia effect on the flow near the upper boundary. A small amount of fluid is pulled up towards the left corner due to drag force created by the motion of the upper lid. The clockwise circulation is found to be more as compared to anticlockwise circulation. As a result, the stream function contours nearer to the upper lid are not exactly oval and two asymmetric rolls with clockwise and anti-clockwise circulations are observed. The magnitude of the stream function is also very low and heat transfer is conduction dominated within the cavity. Due to dominant conduction mode, all the isotherms except $\theta = 0.1$ are smooth symmetric curves that span the entire cavity. The isotherm with $\theta = 0.1$ also occurs symmetrically near the side walls of the enclosure. Fig. 2(b) shows the contour plots for $Gr = 10^4$. Here the effect of lid driven flow tends to vanish and both anticlockwise and clockwise circulations become almost symmetric. The larger value of Gr increases the strength of buoyancy and hence the strength of natural convection within the cavity increases. It is interesting to observe that the strength of circulation increases from 0.15 to 1.5 at the center of the cavity. The streamlines at the center of the cavity are mostly elliptic in shape and far away from the center are rectangular in shape. The isotherms except with $\theta = 0.1$ are smooth curves which span the entire enclosure and they are symmetric with respect to the vertical center line. This also illustrates a conduction dominated effect. Fig. 2(c) shows the effect for $Gr = 10^5$. The larger strength of circulation in this case indicates that buoyancy driven circulation is enhanced inside the cavity. The isotherm contours with $\theta = 0.1$ gradually get shifted towards the vertical wall due to stronger buoyancy effects.

Figs. 3 (a)–(c) show the stream function and temperature contour for various Gr with $Pr = 0.7$ and $Re = 1$. Fig. 3(a) displays the effect of lid driven flow inside the cavity for $Gr = 10^3$. Similar to Fig. 2(a), the strength of clockwise circulation is stronger than the anticlockwise circulation as the lid driven effect dominates over the strength of buoyancy. It is interesting to observe that the temperature distributions are coupled with stream functions for $Pr = 0.7$ and hence the isotherms gradually tend to be asymmetric. Fig. 3(b) shows the contour plots for $Gr = 10^4$. Similar to Fig. 2(b), the effect of lid driven flow gradually diminishes with the increase of Gr. The circulation near the central region becomes stronger and consequently, the temperature contours with $\theta = 0.1$–0.3 start getting shifted towards the side walls (see Fig. 3(b)). The presence of significant convection is also exhibited in other temperature contour lines which start getting deformed and lifted towards the top plate. Fig. 3(c) illustrates contours for $Gr = 10^5$ where both the anticlockwise and clockwise circulations are observed to be symmetric. The effect of lid-driven flow totally vanishes for higher value of Gr as the buoyancy becomes the dominant force due to increase in the value of Gr. The temperature gradients near both the bottom and side walls tend to be significant leading to the development of thermal boundary layer. Fig. 3(b) shows that the weak thermal boundary layers along side walls and the bottom wall occupy nearly 85% of the cavity for $Gr = 10^4$ whereas for $Gr = 10^5$ the isotherms presented in Fig. 3(c) indicate the presence of strong thermal boundary layers occupying about 70% of the cavity. It may be noted that overall thermal boundary layers are based on along two side walls and the bottom wall.

Figs. 4 (a)–(c) display the effect of Gr varying within 10^3 to 10^5 and for $Pr = 10$. It is interesting to observe that the isotherms with $\theta \leqslant 0.4$ are clustered towards the top portion of the right wall illustrating that the convection plays a dominant role in the heat transfer and that contrast the cases for fluids with smaller Pr under identical Gr. As the anti-clockwise circulation cells in the right half are stronger, the isotherms are found to be clustered towards the right wall. Due to higher intensity of circulations, the thermal mixing is larger near the center and the temperature (θ) near the central core varies within 0.4–0.6 (see Fig. 4(a)). The dominant effect of lid velocity is still observed for $Gr = 10^4$ as seen in Fig. 4(b). The circulation cells still show asymmetric trend and the intensity of circulation in the right half is found to be stronger. The effect of natural convection is found to be important for $Gr = 10^4$ and the isotherms with $\theta \leqslant 0.4$ are highly clustered near the walls. It is interesting to observe that the isotherms near both the side walls are symmetric whereas the effect of asymmetric flow is reflected for isotherms near the center (see Fig. 4(b)). The thermal mixing is more for $Gr = 10^4$, and a large region at the center remains at $\theta = 0.4$–0.5. At $Gr = 10^5$, the natural convection dominates the flow and the circulation is found to be symmetric (see Fig. 4(c)). Similar situations were also found for $Gr = 10^5$ as seen in Figs. 2(c) and 3(c). The larger intensity of flow enhances the mixing and the isotherms are highly clustered towards the side walls. A large region at the central core is maintained with

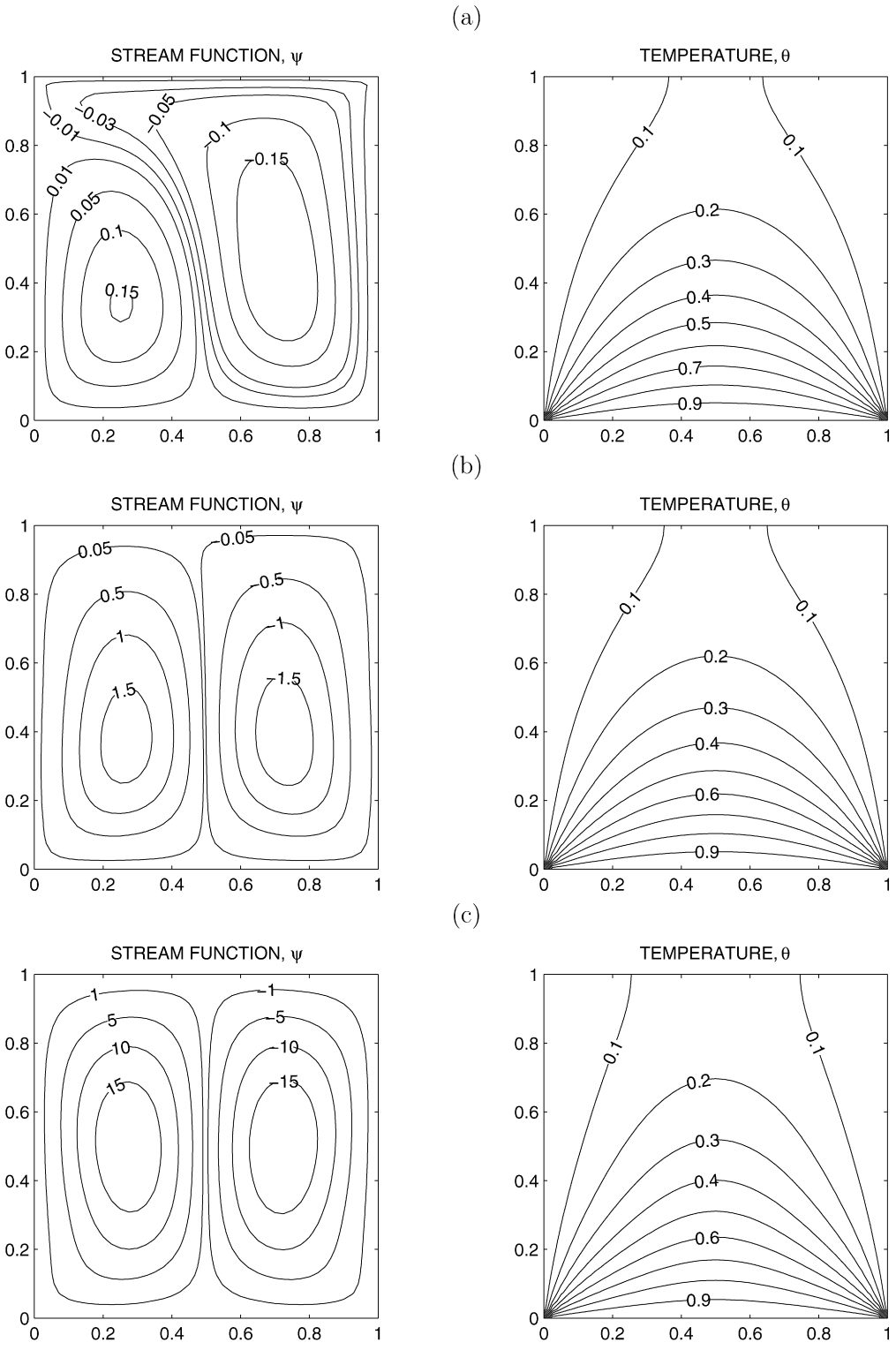

Fig. 2. Stream function and temperature contours for uniform bottom heating case with $Pr = 0.015$, $Re = 1$: (a) $\mathrm{Gr} = 10^3$, (b) $Gr = 10^4$, and (c) $Gr = 10^5$.

$\theta = 0.4$–0.5. The isotherms are found to be symmetric due to dominant natural convection for $Gr = 10^5$.

Streamlines and isotherms for non-uniform bottom heating have also been studied for $Gr = 10^3$–10^5, $Re = 1$ with $Pr = 0.7$ (see Fig. 5) and 10 (see Fig. 6). It has been seen earlier that uniform heating of the bottom wall causes finite discontinuity in the Dirichlet boundary conditions for the temperature distribution at the edges of the bottom wall. In contrast, the non-uniform heating removes singularity at the edges of the bottom wall and provides a smooth temperature distribution in the entire cavity. The circulation pattern as seen in Figs. 5 (a)–(c) is qualitatively similar to that of uniform

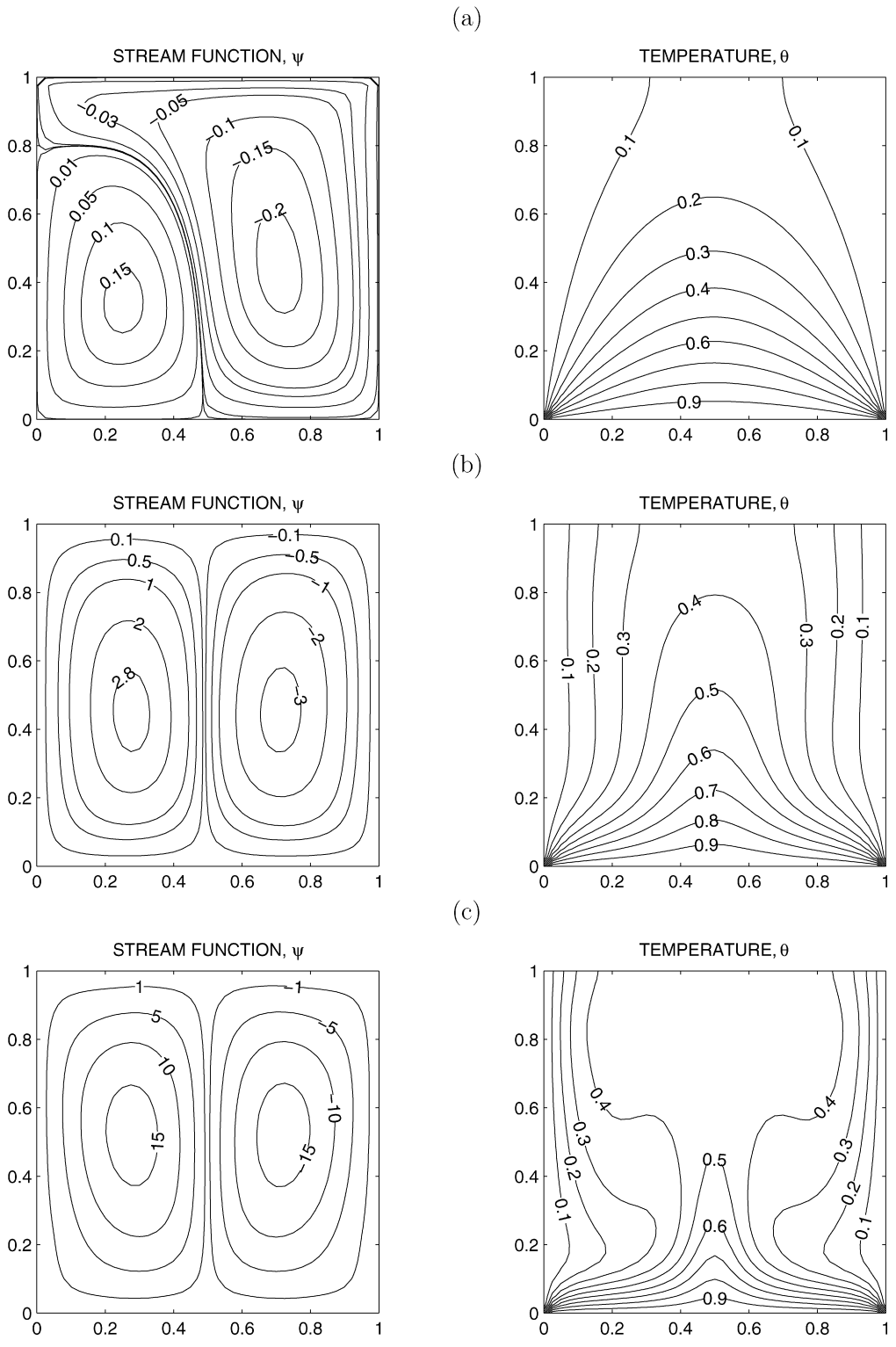

Fig. 3. Stream function and temperature contours for uniform bottom heating case with $Pr = 0.7$, $Re = 1$: (a) $Gr = 10^3$, (b) $Gr = 10^4$, and (c) $Gr = 10^5$.

heating case as seen in Figs. 3 (a)–(c). Due to non-uniform heating, the heating rate near the side wall is generally lower and the temperature decreases from the middle of the bottom wall towards the top and side walls. The isotherms are found to be symmetric with respect to the vertical centerline as seen in Fig. 5(a). The isotherms with $\theta \leqslant 0.2$ occur symmetrically near the side walls for $Gr = 10^4$ (see Fig. 5(b)) and the isotherms with $\theta \leqslant 0.3$ occur symmetrically near the side walls for $Gr = 10^5$ (see Fig. 5(c)). These show the overall lower heating rates which contrast the cases with uniform heating effect (see Figs. 3 (a)–(c)). The streamlines and the isotherms for $Pr = 10$ with non-uniform heating effects are illustrated in

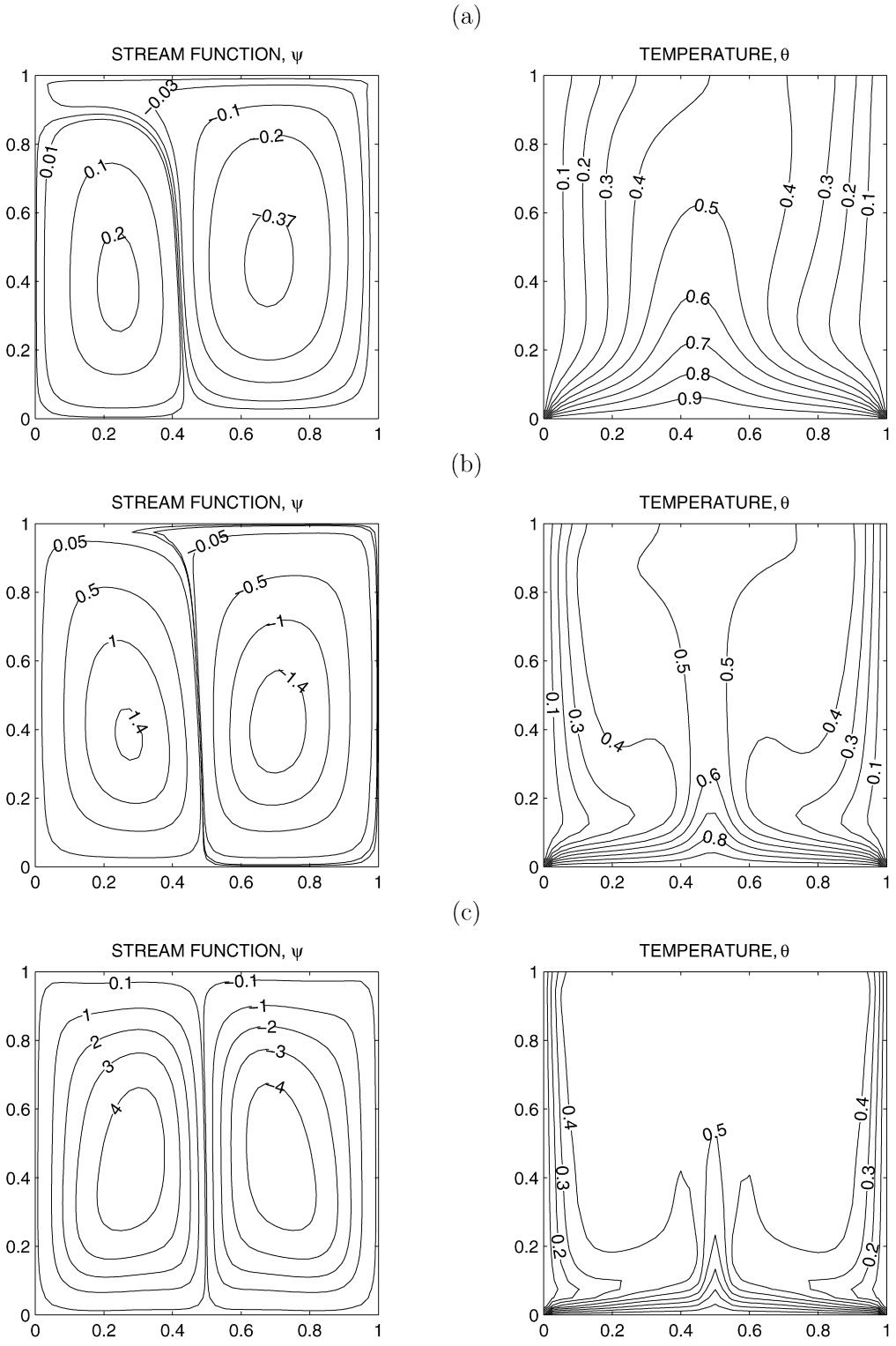

Fig. 4. Stream function and temperature contours for uniform bottom heating case with $Pr = 10$, $Re = 1$: (a) $Gr = 10^3$, (b) $Gr = 10^4$, and (c) $Gr = 10^5$.

Figs. 6 (a)–(c). The circulation patterns are qualitatively similar to that of Fig. 4, but the intensity of circulation is less due to non-uniform heating effects. The isotherms except at the central region are also qualitatively similar to that of Figs. 4 (a)–(c). The temperature of the core is less due to non-uniform heating effect.

4.3. Effect of Reynolds number: uniform and non-uniform heating of the bottom wall

Figs. 7 and 8 display the stream function and isotherm contours for $Re = 1$, 10 and 10^2 with $Gr = 10^3$ corresponding to $Pr = 0.015$ (see Fig. 7) and 10 (see Fig. 8) with uniform bot-

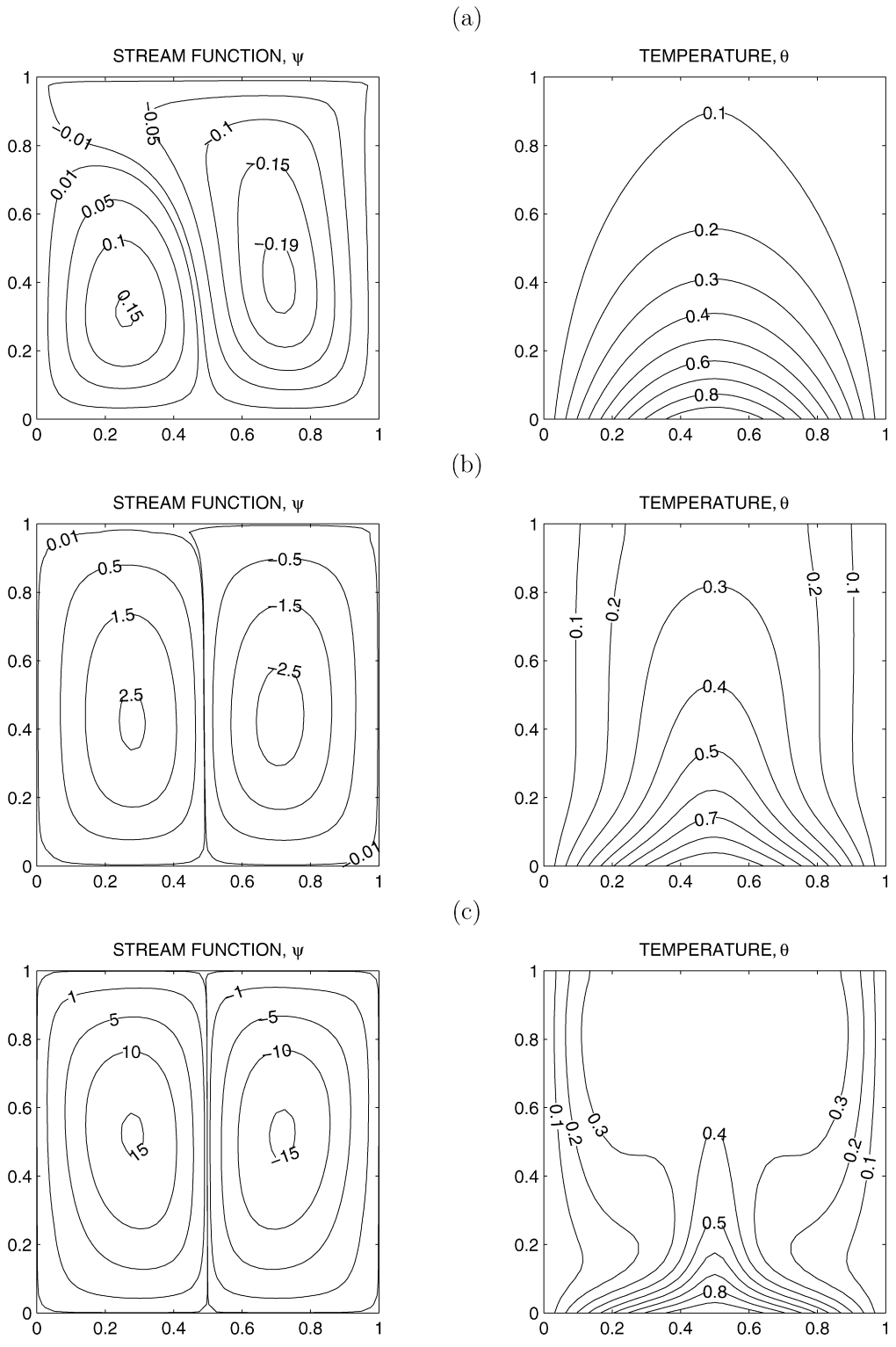

Fig. 5. Stream function and temperature contours for non-uniform bottom heating case with $Pr = 0.7$, $Re = 1$: (a) $Gr = 10^3$, (b) $Gr = 10^4$, and (c) $Gr = 10^5$.

tom heating. The increase in Re enhances the effect of forced convection and suppresses the effect of natural convection. This can also be explained by introducing another dimensionless parameter $Ri = Gr/Re^2$.

Figs. 7 (a)–(c) show the distributions for $Pr = 0.015$ and $Gr = 10^3$ with various values of Re. Fig. 7(a) displays the distributions for $Re = 1$ and $Ri = 10^3$ which denotes a combined effect of buoyancy and lid-driven force inside the cavity. The clockwise and anticlockwise circulations are not symmetric due to additional force created by the motion of the upper lid. The right vortex (primary vortex) is dominant due to movement of the upper wall and the left vortex (secondary vortex) is formed

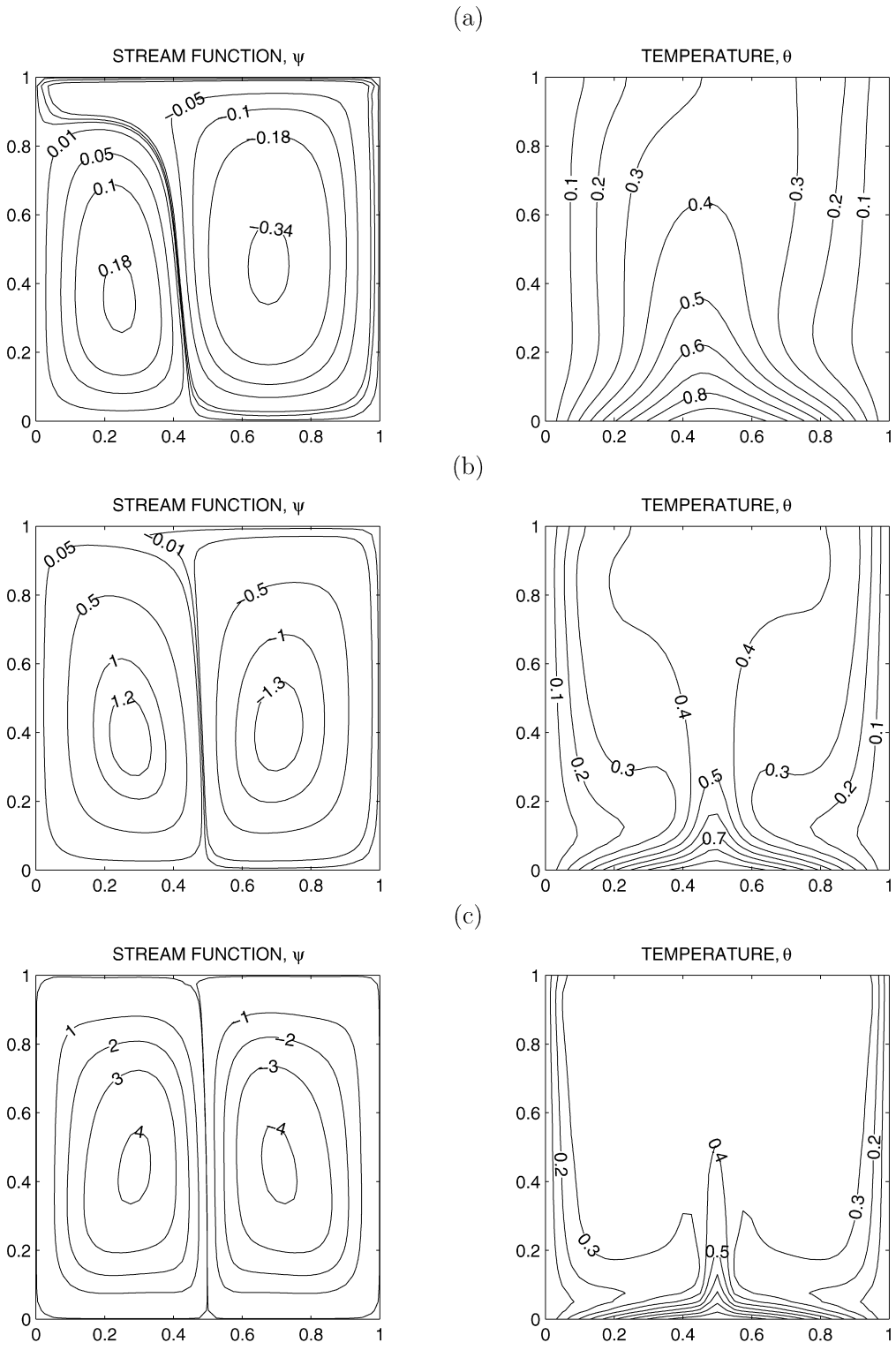

Fig. 6. Stream function and temperature contours for non-uniform bottom heating case with $Pr = 10$, $Re = 1$: (a) $Gr = 10^3$, (b) $Gr = 10^4$, and (c) $Gr = 10^5$.

due to natural convection. It may be noted that on the right wall, the buoyancy and shear forces are in the same direction whereas on the left wall they are opposing each other. Less energy is noticed to be carried away from the sliding top wall into the cavity and, subsequently, the conduction heat transfer regime has become the dominant mode of energy transport in the cavity. All the isotherms except $\theta = 0.1$ span the entire enclosure and they are symmetric with respect to vertical center line. The isotherm $\theta = 0.1$ occurs symmetrically near the side wall of the enclosure. The conduction dominance may also be confirmed by the fact that the stream function and temperature contours are not coupled. Fig. 7(b) shows the effect for $Re = 10$ and $Ri = 10$. As

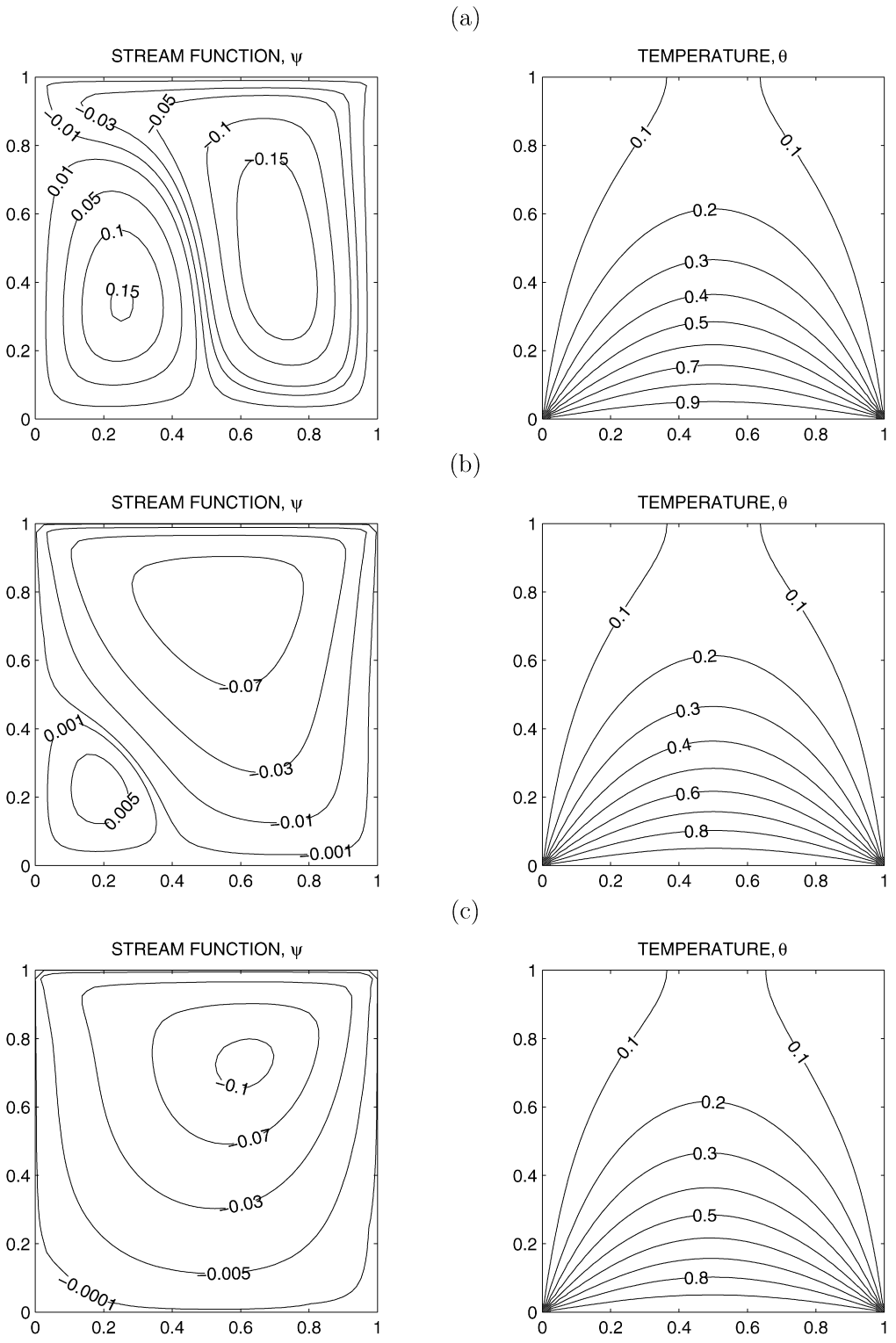

Fig. 7. Stream function and temperature contours for uniform bottom heating case with $Pr = 0.015$, $Gr = 10^3$: (a) $Re = 1$, (b) $Re = 10$, and (c) $Re = 10^2$.

Ri decreases, the effect of buoyancy gradually becomes weaker as compared to the lid driven force. The secondary circulation occupies a very small portion of the bottom left corner and the primary circulation occupies the major portion of the cavity. For $Ri = 0.1$ (see Fig. 7(c)), the circulation pattern resembles the case of lid-driven cavity problem. The secondary circulation vanishes and the primary circulation occupies the entire cavity. The effect of buoyancy almost vanishes in this case. The isotherms illustrate that streamlines and isotherms are decoupled and heat transfer is conduction dominant.

Fig. 8 shows the distributions for higher Prandtl number fluid ($Pr = 10$) with $Re = 1$, 10, 10^2 and $Gr = 10^3$. Fig. 8(a) shows

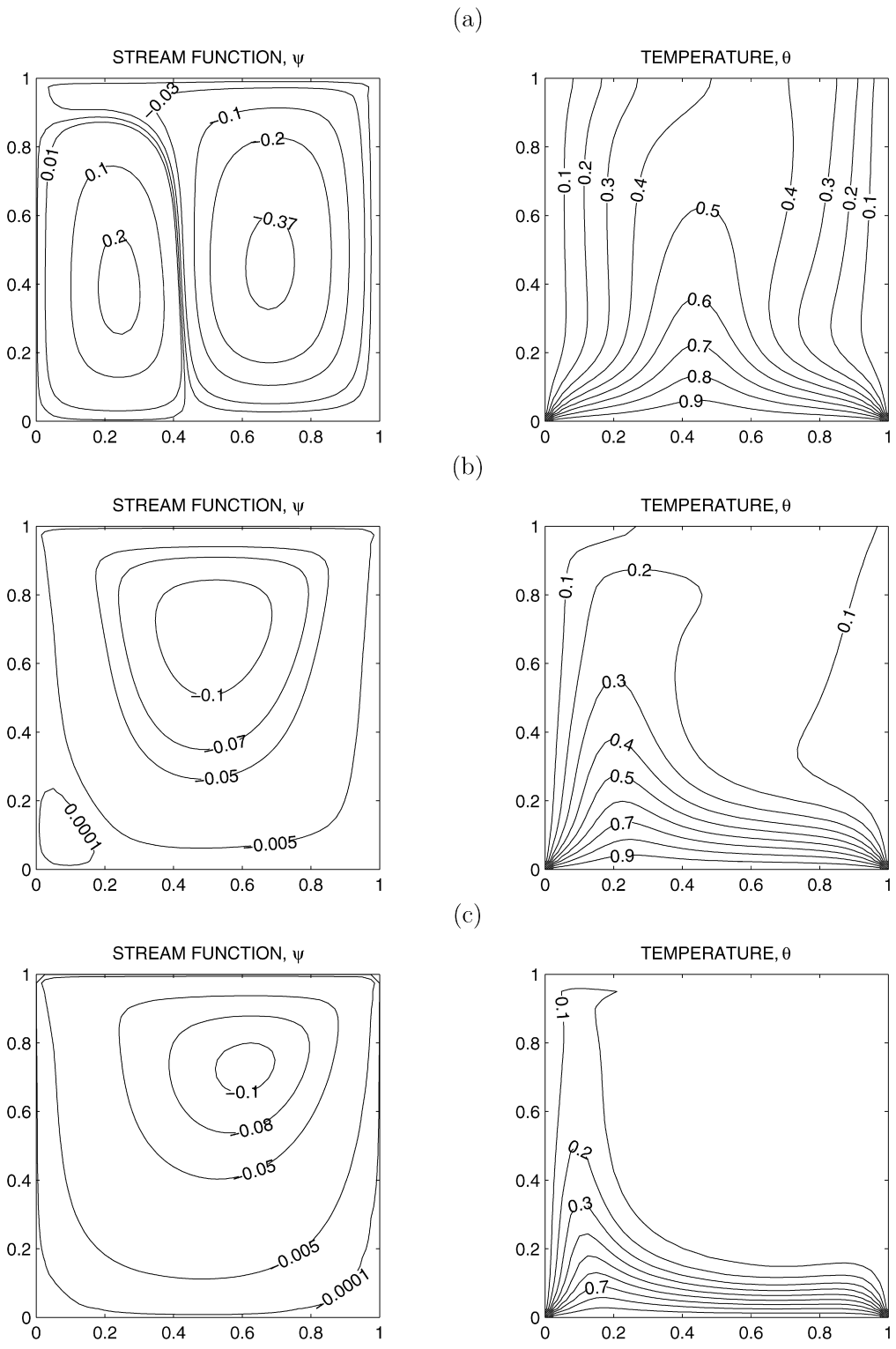

Fig. 8. Stream function and temperature contours for uniform bottom heating case with $Pr = 10$, $Gr = 10^3$: (a) $Re = 1$, (b) $Re = 10$, and (c) $Re = 10^2$.

that the effect of buoyancy increases with the increase of Pr resulting an increase in the strength of anticlockwise circulation as compared to Fig. 7(a) for lower value of Reynolds number ($Re = 1$). The effect of forced convection also increases the strength of clockwise circulation for higher Prandtl number fluids due to higher viscosity. Thus the overall strength of circulation inside the cavity increases as compared to Fig. 7(a). Here, the effect of forced flow is more dominant as compared to effect of buoyant force. Due to increase in the strength of circulation, heat is transferred mostly due to convection. This is contrary to the previous case where heat is transferred due to conduction (see Fig. 7(a)). The temperature gradient near the

bottom walls increases and the isotherms start shifting from the right cold wall. As the value of Re increases to 10, the secondary circulation near the left wall tends to vanish and the primary circulation occupies the entire cavity (see Fig. 8(b)). It is clear from the temperature profile that with the increase in the value of Pr the upper portion of the right half is thermally well mixed and θ is within 0.1–0.2. Since a larger region is isothermally cold, the effect of buoyancy is limited to boundary layers which decreases the strength of secondary vortex as compared to lower value of Re (see Figs. 8 (a), (b)). As Re increases further to 10^2, the flow will transform to a lid-driven cavity flow (see Fig. 8(c)). It is observed that a large region near the right half becomes isothermally cooled and the effect of heating will be confined only near the bottom and left walls of the cavity forming a strong thermal boundary layer attached to the bottom wall occupying only 30% of the cavity.

Fig. 9 displays the effect of Re for $Pr = 10$ and $Gr = 10^3$ for the non-uniform bottom heating. In this case due to absence of discontinuity in heating effects at edges, the isotherms are smooth and continuous curves throughout the entire cavity. The strength of circulation decreases in this case as compared to Fig. 8 due to decrease in heating rates for the non-uniform heating case. The isotherms for $\theta \leqslant 0.4$ occur near both sides of the cavity for the uniform heating while for the non-uniform case the isotherms for $\theta \leqslant 0.3$ occur near the side walls. As the value of Re increases, the inertial force becomes dominant and the flow becomes a lid-driven flow. The heating effects are qualitatively similar as seen in Figs. 8(b) and 9(b) as well as Figs. 8(c) and 9(c). A larger cold region near the right wall is observed as seen in Fig. 9(c) and the region is larger due to non-uniform heating at the bottom wall.

4.4. Effect of Prandtl number: uniform and non-uniform heating of the bottom wall

The effect of Pr for representative higher values of Re and Gr has been illustrated in Figs. 10–12. Although Ri is fixed in each case, the figures show that the flow inside the cavity is a function of Pr. It is interesting to observe that either conduction, or natural convection or forced convection is dominant for various values of Pr with $Ri = 100$ in presence of uniform heating of bottom wall (see Figs. 10 (a)–(c)). The isotherms illustrate conduction dominance at $Pr = 0.015$ with the maximum value of stream function being 0.2. It is interesting to observe that the right circulation cells are dominant which signify that the forced convection, however weak, is gradually developed and the conduction dominant heating effect is observed due to less intense circulations (Fig. 10(a)). The flow circulations are qualitatively similar for $Pr = 0.7$. The maximum value of stream function for the right circulation cell is 0.4 and the size of the right circulation cells is larger than that with $Pr = 0.015$. Due to enhanced circulation and thermal mixing at the right half, the isotherms are pushed towards the left-side wall. The dominant forced convection is attributed to the asymmetric isotherms as seen in Fig. 10(b). The primary circulation occupies most of the cavity except a smaller cell consisting of secondary circulations occurring near the left wall for $Pr = 10$ (Fig. 10(c)). The enhanced thermal mixing due to large intense primary circulation near the right half leads to the temperature varying within 0.4–0.5 near the right wall. A thin boundary layer is found to occur along the top portion of the right wall whereas the isotherms are pushed near the left wall. Isotherms are also pushed towards the bottom wall due to large primary circulation cells. Thus strong thermal boundary layers are also formed along the left and bottom walls. It is also interesting to observe that isotherms near the left wall are non-monotonic due to occurrence of the secondary cells.

Figs. 11 (a)–(c) illustrate the stream function and isotherm contours for $Re = 10$ and $Gr = 10^4$ with various Pr in presence of non-uniform heating. The qualitative trends of primary and secondary cells are similar to that with uniform heating effect as seen in Figs. 10 (a)–(c). The conduction dominant heating effect is observed for $Pr = 0.015$ (see Fig. 11(a)) similar to uniform heating case. The convection dominant heating effects are observed for $Pr = 0.7$ and 10 and similar to uniform heating situation, the strong thermal boundary layer is found to develop near the left wall and the central region of the bottom wall for $Pr = 10$. It is interesting to observe that the temperature gradient is larger at the central region of the bottom wall due to the non-uniform heating effect for all Prandtl numbers.

Figs. 12 (a)–(c) illustrate the stream function and temperature contours for $Re = 10^2$ and $Gr = 10^4$ with various Pr in presence of uniform heating of the bottom wall. It may be noted that, $Ri = 1$ for all the cases and it is interesting to observe that primary circulation cells almost occupy the entire cavity. It is also observed that secondary circulation cells appear near the left corner of the bottom wall and the secondary cell disappears at $Pr = 10$. Fig. 12(a) shows that the temperature distributions are weakly coupled with stream function for $Pr = 0.015$ and hence the isotherms tend to be symmetric resulting in conduction dominated flow. As Pr increases to 0.7, the isotherms are clustered towards the bottom and left walls and convection plays a dominant role in heat transfer. For further increase of Pr to 10, the compression of isotherms are more prominent and a strong thermal boundary layer develops near the bottom and left wall (see Fig. 12(c)). Due to the compression of isotherms towards the left wall, the heat transfer rates through the bottom and left walls are more as compared to the right wall. Similar effects are also observed for non-uniform heating of the bottom wall.

4.5. Heat transfer rates: local and average Nusselt numbers

Figs. 13 (a)–(c) show the heat transfer rates (Nu_b, Nu_r and Nu_l) for various Pr. The heat transfer rate (Nu_b) is very high at the edges of the bottom wall due to discontinuities present at the edges for uniform heating case and Nu_b reduces towards the center of the bottom wall. The heat transfer rate is minimum near the central region due to less temperature gradient for all Pr as seen in Figs. 10 (a)–(c). It is observed that the local minima for $Pr = 0.015$ is lesser than that for $Pr = 0.7$. It is also interesting to observe that Nu_b is almost flat over a large region near the center for $Pr = 0.7$ and that is due to the occurrence of dispersed isotherm contours. The smaller heat transfer rate

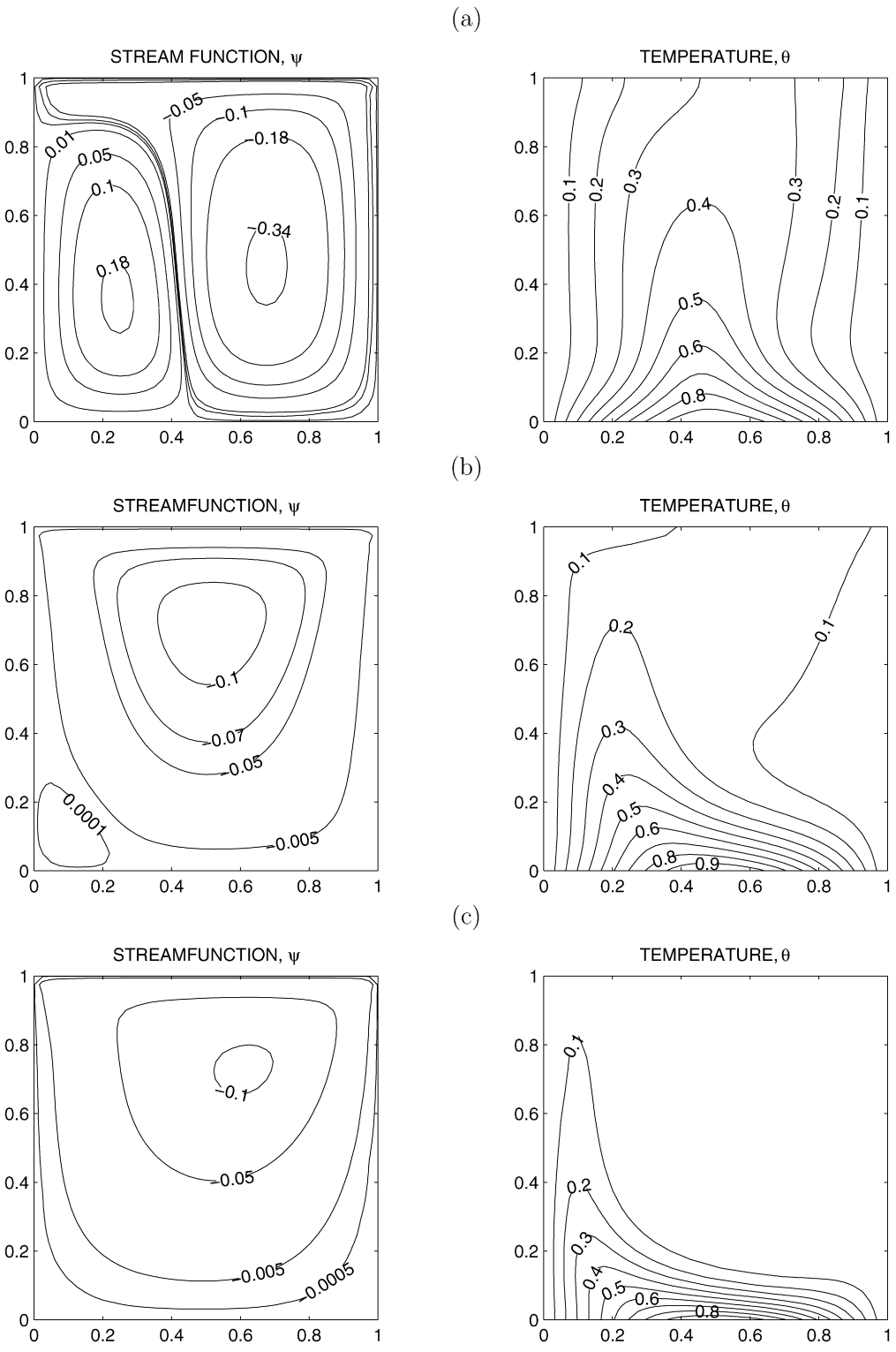

Fig. 9. Stream function and temperature contours for non-uniform bottom heating case with $Pr = 10$, $Gr = 10^3$: (a) $Re = 1$, (b) $Re = 10$, and (c) $Re = 10^2$.

(Nu_b) at $X = 0.4$ is observed due to the presence of secondary flow and stagnation point which result in less heat transfer causing smaller temperature gradient as seen in Fig. 10(b). The enhanced thermal mixing occurs for $Pr = 10$ and the isotherms are highly clustered near the right portion of the bottom wall, but the minima in Nu_b occurs near $X = 0.3$ due to the flow separation as seen in Fig. 10(c). It may be interesting to note that the flow separation does not influence the thermal gradient for $Pr = 0.015$ due to the conduction dominant heat transfer.

The local heat transfer rates (Nu_b) are also shown for non-uniform heating cases (see Fig. 13(a)). The heat transfer rates are lesser at the edges for all Pr as there is no discontinuity in

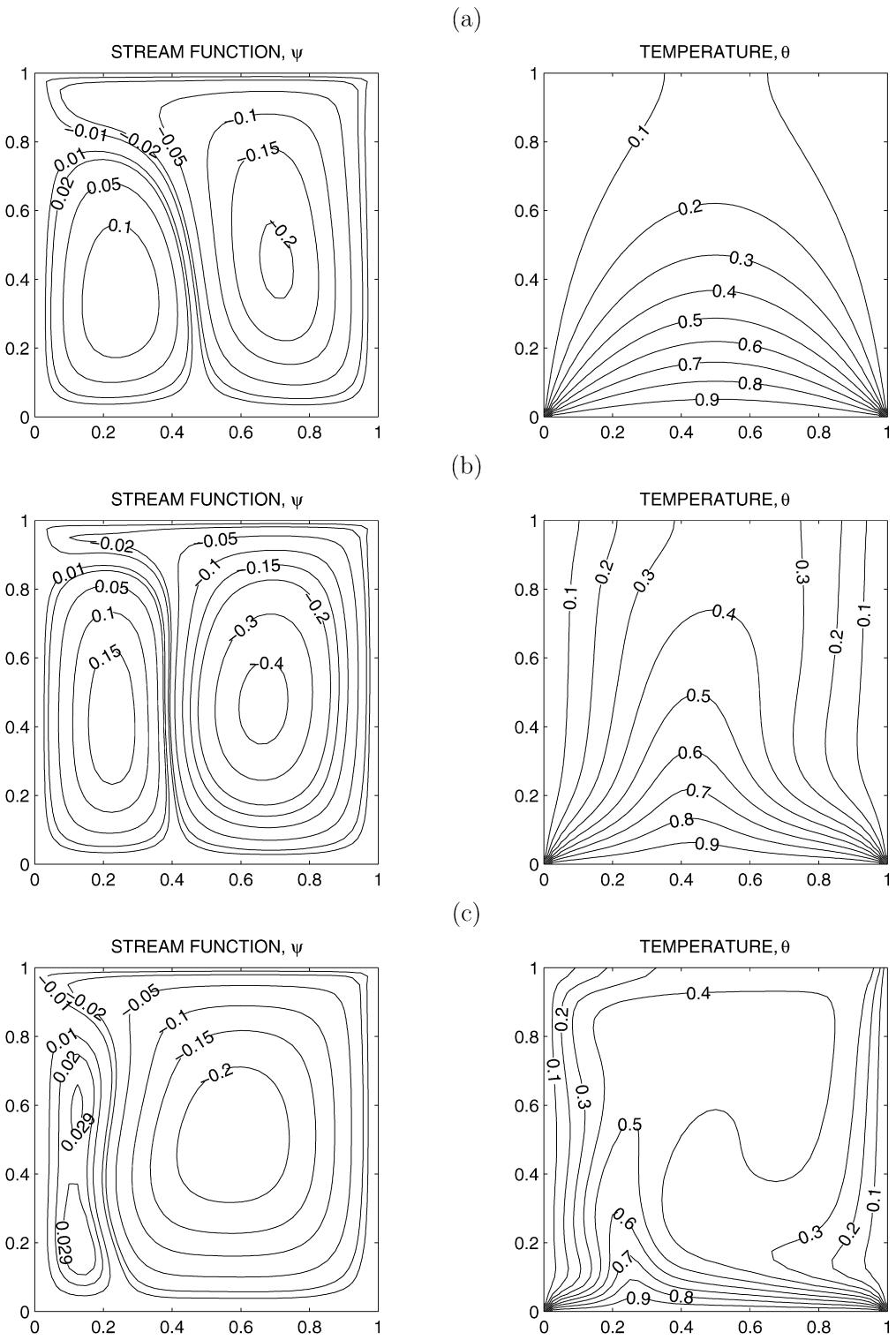

Fig. 10. Stream function and temperature contours for uniform bottom heating case with $Re = 10$, $Gr = 10^4$: (a) $Pr = 0.015$, (b) $Pr = 0.7$, and (c) $Pr = 10$.

temperature for non-uniform heating of the bottom wall. It is observed that Nu_b has local maxima at $X = 0.5$ for $Pr = 0.015$ and symmetric Nu_b vs. X is observed due to conduction dominant heat transfer. Although Nu_b is almost identical at the center for $Pr = 0.015$ and 0.7, but an additional dominant local maxima also occurs at $X = 0.7$ for $Pr = 0.7$ due to compression of isotherms as seen in Fig. 11(b). Two local maxima in Nu_b occur at $X = 0.15$ and 0.65 for $Pr = 10$ as the isotherms are concentrated due to enhanced thermal mixing as seen in Fig. 11(c).

Fig. 13(b) illustrates local heat transfer rate at the right wall (Nu_r) for uniform and non-uniform heating of bottom wall. It

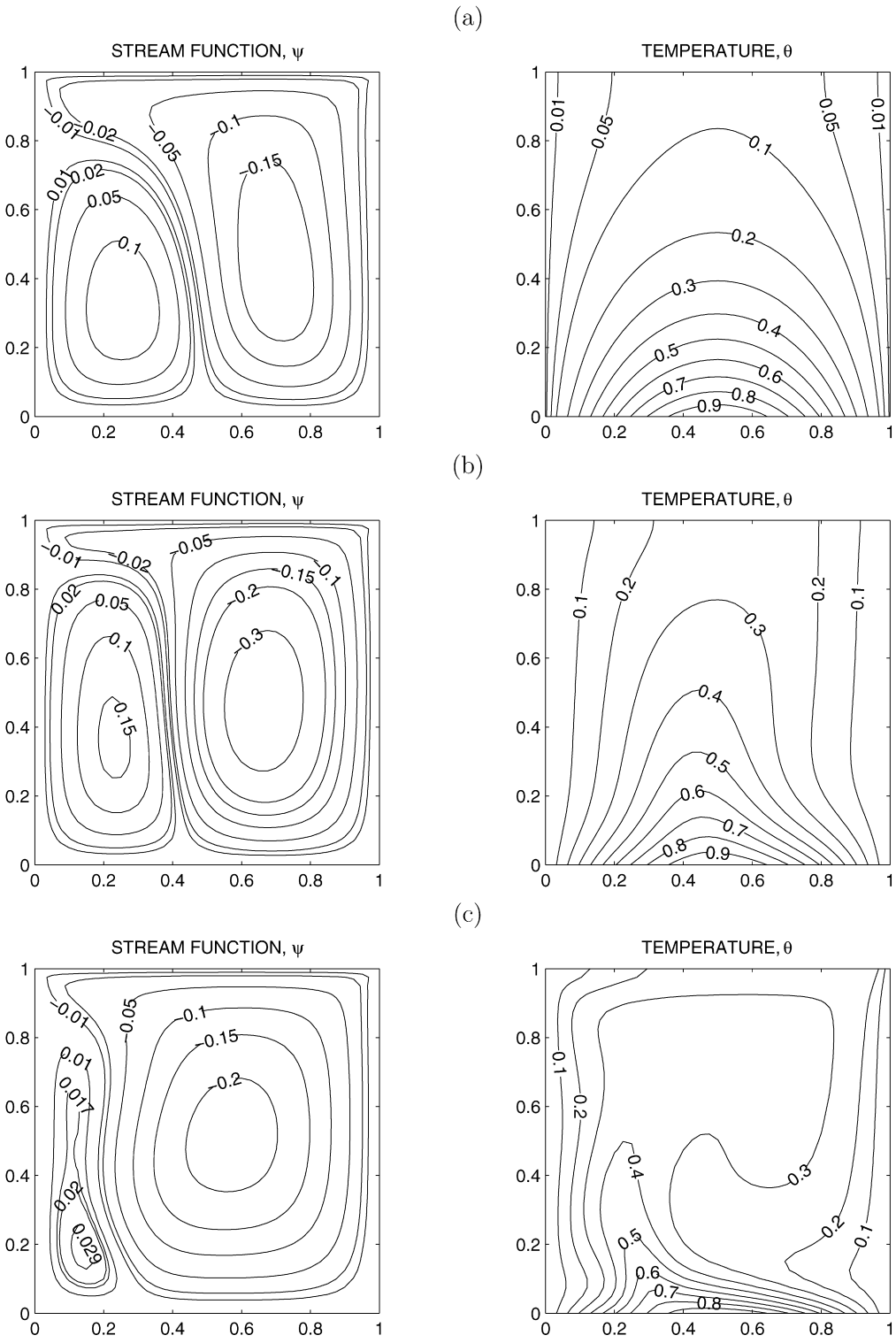

Fig. 11. Stream function and temperature contours for non-uniform bottom heating case with $Re = 10$, $Gr = 10^4$: (a) $Pr = 0.015$, (b) $Pr = 0.7$, and (c) $Pr = 10$.

is observed that Nu_r decreases with vertical distance especially for $Pr = 0.015$ and 0.7 for both uniform and non-uniform heating situations. This is due to the fact that thermal boundary layer starts to grow from the bottom edge and the thickness of the boundary layer is higher at the top of the side wall. As Pr increases to 10, Nu_r takes the minimum value at the bottom of the right wall due to larger thickness of the boundary layer and Nu_r increases with the increase of vertical distance as the isotherms are highly clustered due to larger intensity of flow for both uniform and non-uniform heating effects (see Figs. 11(c) and 12(c)). Although, the qualitative trends of Nu_r distribution for specific Pr are similar with uniform and non-uniform heat-

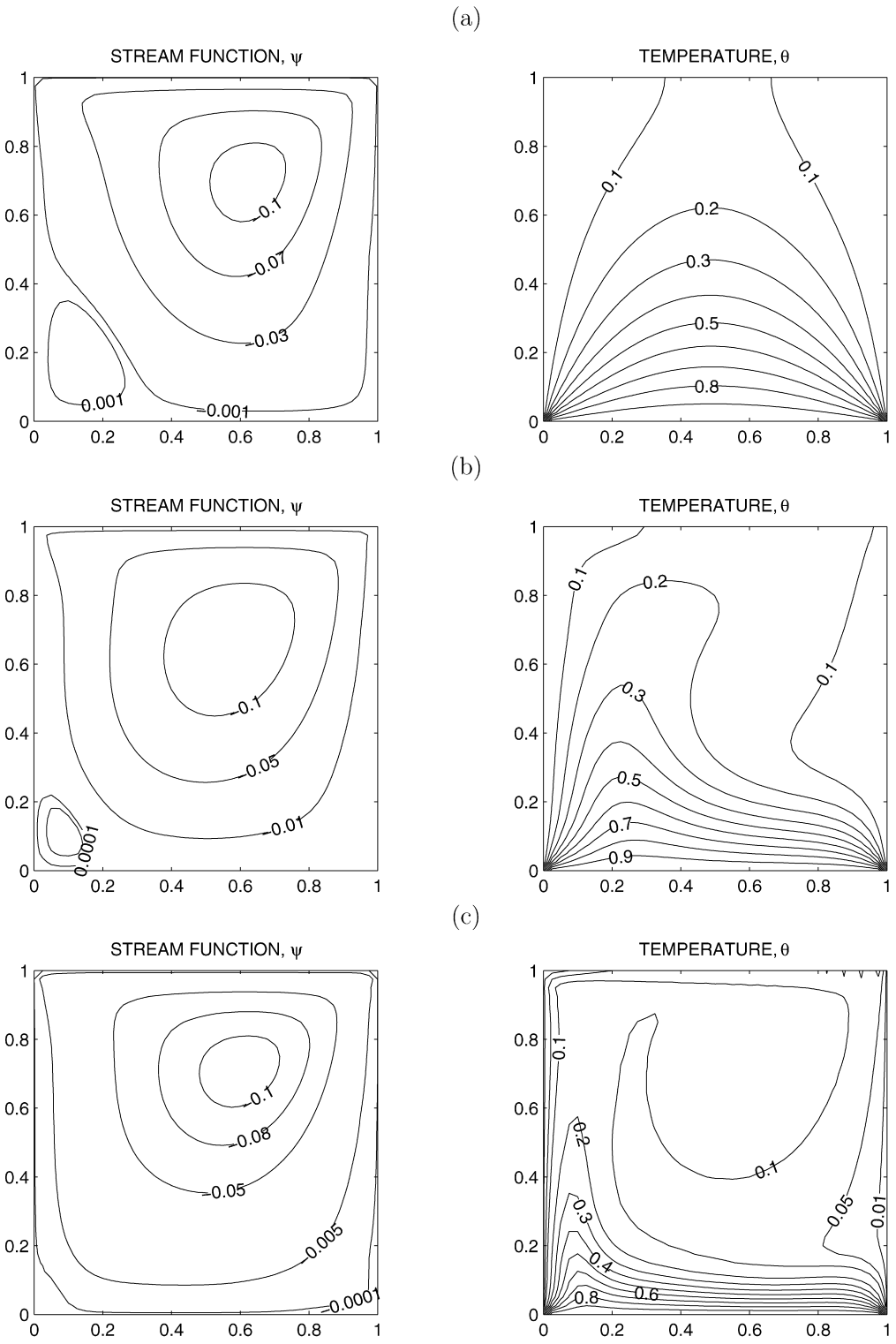

Fig. 12. Stream function and temperature contours for uniform bottom heating case with $Re = 10^2$, $Gr = 10^4$: (a) $Pr = 0.015$, (b) $Pr = 0.7$, and (c) $Pr = 10$.

ing situations, but Nu_r is smaller due to non-uniform heating effect at a specific location.

Variations of local heat transfer rates at the left wall (Nu_l) are shown in Fig. 13(c). It is observed that Nu_l is found to decrease with the distance for $Pr = 0.015$ and 0.7 for both uniform and non-uniform heating situations and similar trends were observed for variations of Nu_r. In contrast, Nu_l shows non-monotonic behavior with distance and two intermediate maxima in Nu_l occurs for $Pr = 10$ due to both uniform and non-uniform heating of the wall. This non-monotonic variation of Nu_l is due to wavy distributions of isotherms near the left wall resulting from multiple secondary circulations.

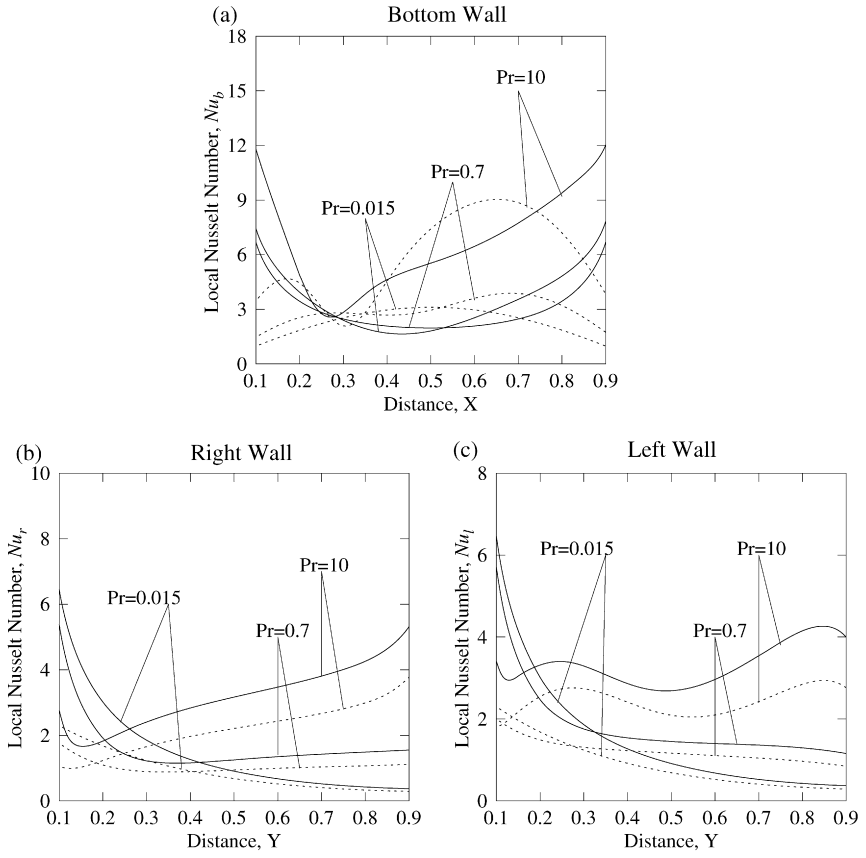

Fig. 13. Variation of local Nusselt number with the distance at the (a) bottom wall, (b) right wall, and (c) left wall for uniform heating (—) and non-uniform heating (...) for $Gr = 10^4$ and $Re = 10$.

Figs. 14 (a)–(c) display the distributions for local Nusselt number for $Re = 10^2$. The distributions of Nusselt numbers for $Pr = 0.015$ with $Re = 10^2$ are similar to the distributions with $Re = 10$ in presence of uniform and non-uniform heating effects. Due to increase in the value of Re, the effect of inertia increases and isotherms are pushed towards the bottom and left wall as observed for $Pr = 0.7$ and 10 (see Figs. 12 (b), (c)). It is interesting to observe that the intensity of circulations near the left corner is less and secondary circulation may appear near the left corner. As a result, the thermal mixing is less and thus the thermal gradient is less near the left corner of the bottom wall due to uniform heating effects. Thereafter, Nu_b increases along the bottom wall. Note that, qualitatively similar Nu_b distributions for non-uniform heating cases are observed with $Re = 10$ and $Re = 10^2$ (see Figs. 13(a) and 14(a)).

Fig. 14(b) represents the distributions of Nu_r for all Pr and the distributions are qualitatively similar to those for $Re = 10$. However, Nu_r at the top portion is lesser for $Re = 10^2$ especially with larger Pr due to enhanced thermal mixing in presence of uniform and non-uniform heating effects. Variations of Nu_l are shown in Fig. 14(c). Due to enhanced convection and thermal mixing, the thickness of the boundary layer near the bottom of the left wall is quite less especially for $Pr = 10$ with uniform heating case. As a result, the local heat transfer rate (Nu_l) is quite large near the bottom portion of the left wall. The enhancement of heat transfer rate with smaller magnitude is also observed for non-uniform heating effects. It is interesting to note that Nu_l was oscillatory for $Re = 10$ as seen in Fig.13(c) due to secondary circulations whereas the strong primary circulation for $Pr = 10$ cause the monotonic trend in Nu_l as seen in Fig. 14(c).

The overall effects on heat transfer rates are shown in Figs. 15 (a)–(d), where the distributions of the average Nusselt number at bottom and side walls, respectively, are plotted versus logarithmic Grashof number. The average Nusselt numbers are obtained using Eqs. (17) and (18) where the integral is evaluated using Simpson's 1/3 rule. Figs. 15 (a) and (b) display uniform heating case and Figs. 15 (c) and (d) represent non-uniform heating case. For all these cases, it is observed that average Nusselt numbers for the bottom and side walls remain constant for $Pr = 0.015$. This is due to the fact that the conduction is dominant for lower value of Pr irrespective of Gr. The average Nusselt number remains constant upto $Gr = 5 \times 10^3$ for both uniform and non-uniform heating case with $Pr = 0.7$ and thereafter average Nusselt number increases. At $Pr = 10$, the average Nusselt number for the left wall shows a kink at $Gr = 10^4$, due to non-monotonic behavior of Nu_l as shown in Fig. 13(c). On the other hand, the average Nusselt number for the right wall shows an inflexion point at $Gr = 10^4$ and average Nusselt number increases slowly beyond $Gr = 10^4$ and $Pr = 10$. This is due to large degree of compression of isotherms near the left and bottom walls and enhanced thermal mixing near the right wall. Due to higher degree of compression of isotherms especially at higher Gr, the power law correla-

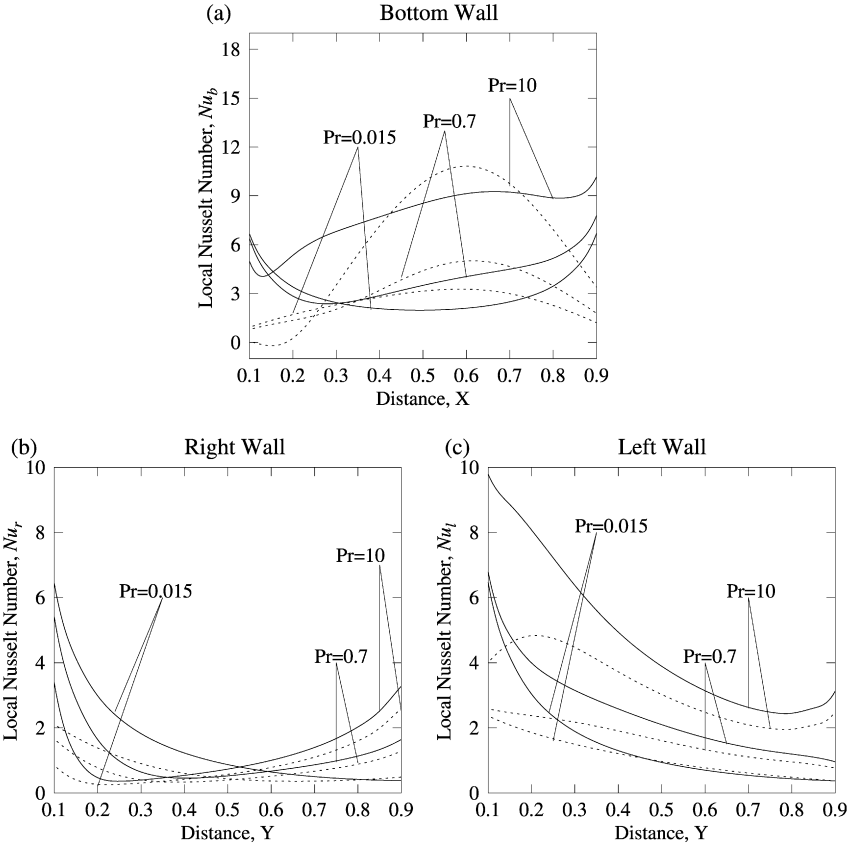

Fig. 14. Variation of local Nusselt number with the distance at the (a) bottom wall, (b) right wall, and (c) left wall for uniform heating (—) and non-uniform heating (...) for $Gr = 10^4$ and $Re = 10^2$.

tion between average Nusselt number and Grashof number may not be obtained and this can be further attributed to kink and inflexion points in average Nusselt number curves as seen in Figs. 15 (b) and (d).

5. Conclusions

The prime objective of the current investigation is to study the effect of uniform and non-uniform heating of the bottom wall on the flow and heat transfer characteristics due to lid driven mixed convection flows within a square cavity. It is evident that for fixed *Re* and *Pr*, the strength of circulation increases with the increase in *Gr*. As *Gr* increases, the effect of buoyancy increases leading to an increase in the strength of circulation. Due to increase in circulation strength, the isotherms are stretched along the side walls and heat is transferred mostly by convection for higher value of *Pr*. The effect of *Re* has also been studied in the present investigation for fixed value of *Pr* and *Gr*. It is observed that the effect of natural convection decreases and forced convection increases with the increase of *Re*. It has also been observed that for higher value of *Pr*, the effect of heating is more pronounced near the bottom and left walls as the formation of thermal boundary layers is restricted near the bottom and left wall for both uniform and non-uniform heating cases. Two circulation cells and one circulation cell are observed for mixed convection and forced convection situations, respectively irrespective of *Pr*. It may be noted that two symmetric circulation cells were found during natural convection with identical boundary conditions [28]. The unique circulation cells are found to be stable which is tested via various initial guesses for Newton–Raphson method leading to unique solution. It may be important to note that an earlier work is based on multiple flow circulations for the study of Rayleigh Benard configuration [34].

The heat transfer rate is very high at the edges of the bottom wall and it decreases at the center for the uniform heating which is in contrast with lower heat transfer rate at the edges for the non-uniform heating of the bottom wall. The local Nusselt numbers for the bottom and side walls also shows several important features. The local Nusselt number for the bottom wall (Nu_b) increases in the right half of the cavity for the uniform heating whereas for non-uniform heating case it increases towards the center as the effect of heating is maximum at the center. The local Nusselt number plot for the side wall shows that the heat transfer rate for uniform heating is always more as compared to the non-uniform heating. The local Nusselt number (Nu_l) shows oscillatory behavior for $Pr = 10$ and $Re = 10$ whereas Nu_r has a minima at the center and that increases with the increase of vertical distance. The average Nusselt number for the bottom wall ($\overline{Nu_b}$) shows power law variations for *Gr* with higher *Pr*. On the other hand, $\overline{Nu_l}$ shows kink at $Gr = 10^4$ and the variation of $\overline{Nu_r}$ shows an inflexion point at $Gr \geqslant 10^4$. Thus the overall power law correlation for average Nusselt numbers

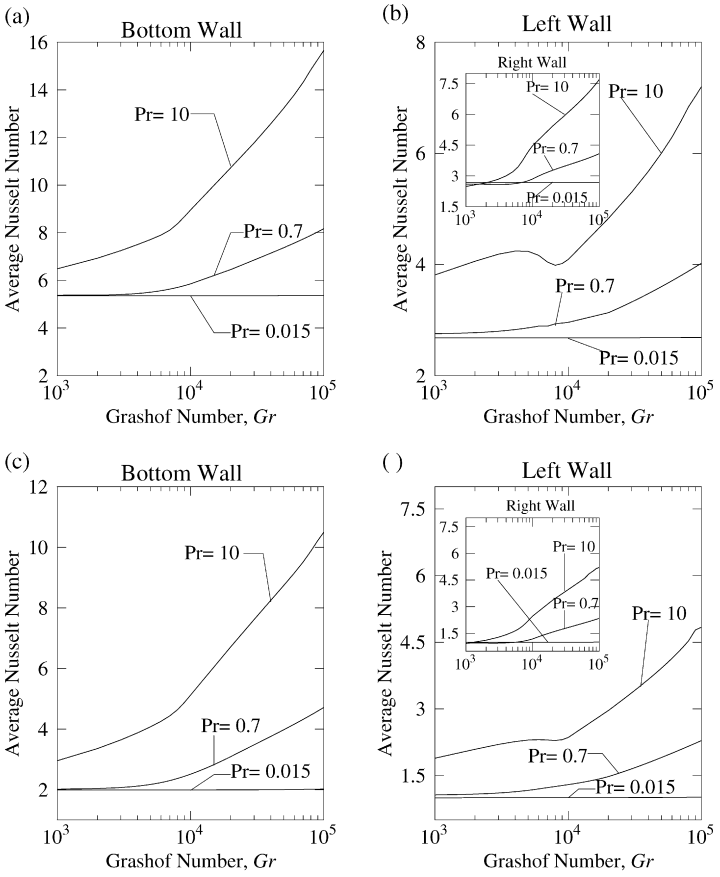

Fig. 15. Variation of average Nusselt number plot with Grashof number for uniform heating [a and b] and for non-uniform heating [c and d] with $Pr = 0.015$, 0.7, and 10 and $Re = 10$.

may not be obtained for mixed convection effects particularly at higher Pr.

Acknowledgement

Authors would like to thank anonymous reviewers for critical comments which improved the quality of the manuscript. Authors also acknowledge the generous help of Dr. Khalil Khanafer for valuable suggestions.

References

[1] A. Bejan, Convective Heat Transfer, Wiley, New York, pp. 141–146.
[2] C.K. Cha, Y. Jaluria, Recirculating mixed convection flow for energy extraction, Int. J. Heat Mass Transfer 27 (1984) 1801–1810.
[3] J. Imberger, P.F. Hamblin, Dynamics of lake reservoirs and cooling ponds, Annu. Rev. Fluid Mech. 14 (1982) 153–187.
[4] F.J.K. Ideriah, Prediction of turbulent cavity flow driven by buoyancy and shear, J. Mech. Engng. Sci. 22 (1980) 287–295.
[5] L.A.B. Pilkington, Review lecture: The float glass process, Proc. R. Soc. Lond. A 314 (1969) 1–25.
[6] R. Schriber, H.B. Keller, Driven cavity flows by efficient numerical techniques, J. Comput. Phys. 49 (1983) 310–333.
[7] M.C. Thompson, J.H. Ferziger, An adaptive multigrid technique for the incompressible Navier–Stokes equations, J. Comput. Phys. 82 (1989) 94–121.
[8] M.K. Moallemi, K.S. Jang, Prandtl number effects on laminar mixed convection heat transfer in a lid-driven cavity, Int. J. Heat Mass Transfer 35 (1992) 1881–1892.
[9] A.K. Prasad, J.R. Koseff, Combined forced and Natural convection heat transfer in a deep lid-driven cavity flow, Int. J. Heat Fluid Flow 17 (1996) 460–467.
[10] A.A. Mohamad, R. Viskanta, Effects of upper lid shear on the stability of flow in a cavity heated from below, Int. J. Heat Mass Transfer 32 (1989) 2155–2166.
[11] A.M. Al-Amiri, K.M. Khanafer, I. Pop, Effect of sinusoidal wavy bottom surface on mixed convection heat transfer in a lid driven cavity, Int. J. Heat Mass Transfer 50 (2007) 1771–1780.
[12] A.A. Mohamad, R. Viskanta, Transient low Prandtl number fluid convection in a lid driven cavity, Numer. Heat Transfer A 19 (1991) 187–205.
[13] C.J. Chen, K.S. Ho, Finite analytical numerical solution of heat transfer in two dimensional cavity flow, Numer. Heat Transfer 4 (1981) 179–197.
[14] K. Torrance, R. Davis, D. Gill, D. Gautam, A. Hsui, S. Lyons, H. Zien, Cavity flows driven by buoyancy and shear, J. Fluid Mech. 51 (1972) 221–231.
[15] R. Iwatsu, J.M. Hyun, K. Kuwahara, Convection in a differentially heated square cavity with a torsionally oscillating lid, Int. J. Heat Mass Transfer 35 (1992) 1069–1076.
[16] R. Iwatsu, J.M. Hyun, K. Kuwahara, Numerical simulation of flows driven by torsionally oscillating lid in a square cavity, J. Fluids Eng. 114 (1992) 143–151.
[17] R. Iwatsu, J.M. Hyun, Three dimensional driven cavity flows with a vertical temperature gradient, Int. J. Heat Mass Transfer 38 (1995) 3319–3328.
[18] A.A. Mohamad, R. Viskanta, Flow and Heat transfer in a lid driven cavity with a stably stratified fluid, Appl. Math. Model. 19 (8) (1995) 465–472.
[19] V.S. Arpaci, P.S. Larsen, Convection Heat Transfer, Prentice-Hall, 1984, p. 90.
[20] A.J. Chamkha, Hydromagnetic combined convection flow in a vertical lid-driven cavity with internal heat generation or absorption, Numer. Heat Transfer A 41 (2002) 529–546.

[21] H.F. Oztop, I. Dagtekin, Mixed convection in two sided lid-driven differentially heated square cavity, Int. J. Heat Mass Transfer 47 (2004) 1761–1769.

[22] O. Manca, S. Nardini, K. Khanafer, K. Vafai, Effect of heated wall position on mixed convection in a channel with an open cavity, Numer. Heat Transfer A 43 (2003) 259–282.

[23] O. Manca, S. Nardini, K. Vafai, Experimental investigation of mixed convection in a channel with an open cavity, Experimental Heat Transfer 19 (2006) 53–68.

[24] O. Manca, S. Nardini, K. Vafai, Experimental investigation of opposing mixed convection in a channel with an open cavity below, Experimental Heat Transfer 21 (2008) 99–114.

[25] E. Papanicolaou, Y. Jaluria, Mixed convection from an isolated heat source in a rectangular enclosure, Numer. Heat Transfer A 18 (1990) 427–461.

[26] T.H. Hsu, P.T. Hsu, S.P. How, Mixed convection in a partially divided rectangular enclosure, Numer. Heat Transfer A 31 (1997) 655–683.

[27] T.H. Hsu, S.G. Wang, Mixed convection in a rectangular enclosure with discrete heat sources, Numer. Heat Transfer A 38 (2000) 627–652.

[28] T. Basak, S. Roy, A.R. Balakrishnan, Effect of thermal boundary conditions on natural convection flow in a square cavity, Int. J. Heat Mass Transfer 49 (2006) 4525–4535.

[29] J.N. Reddy, An Introduction to Finite Element Analysis, McGraw-Hill, New York, 1993.

[30] O.C. Zienkiewicz, R.L. Taylor, J.M. Too, Reduced integration technique in general analysis of plates and shells, International Journal for Numerical Methods in Engineering 3 (1971) 275–290.

[31] S. Roy, T. Basak, Finite element analysis of natural convection flows in a square cavity with non-uniformly heated wall(s), Int. J. Engrg. Sci. 43 (2005) 668–680.

[32] G.K. Batchelor, An Introduction to Fluid Dynamics, Cambridge University Press, 1993.

[33] M.M. Ganzarolli, L.F. Milanez, Natural convection in rectangular enclosures heated from below and symmetrically cooled from the sides, Int. J. Heat Mass Transfer 38 (1995) 1063–1073.

[34] E.H. Ridouane, M. Hasnaoui, A. Amahmid, A. Raji, Interaction between natural convection and radiation in a square cavity heated from below, Numer. Heat Transfer A Applications 45 (3) (2004) 289–311.